Development of phosphoryl-functionalized algal-PEI beads for the sorption of Nd(III) and Mo(VI) from aqueous solutions – Application for rare earth recovery from acid leachates

Yuezhou Wei, Khalid A.M. Salih, Kamal Rabie, Khalid Elwakeel, Yasser Zayed, Mohammed Hamza, Eric Guibal

Development of phosphoryl-functionalized algal-PEI beads for the sorption of Nd(III) and Mo(VI) from aqueous solutions – Application for rare earth recovery from acid leachates

Yuezhou Wei [a,b], Khalid A.M. Salih [a], Kamal Rabie [c], Khalid Z. Elwakeel [d,e], Yasser E. Zayed [f], Mohammed F. Hamza [a,c,*], Eric Guibal [g,*]

[a] Guangxi Key Laboratory of Processing for Non-ferrous Metals and Featured Materials, School of Resources, Environment and Materials, Guangxi University, Nanning 530004, PR China
[b] Shanghai Jiao Tong University, Shanghai, PR China
[c] Nuclear Materials Authority, POB 530, El-Maadi, Cairo, Egypt
[d] Environmental Science Department, Faculty of Science, Port-Said University, Port-Said, Egypt
[e] University of Jeddah, College of Science, Department of Chemistry, Jeddah, Saudi Arabia
[f] Faculty of Science, Menoufia University, Shebine El-Koam, Egypt
[g] IMT – Mines Ales, Polymers Composites and Hybrids (PCH), F-30319 Alès cedex, France

A B S T R A C T

Alginate-PEI beads are functionalized by phosphorylation and applied for the sorption of Nd(III) and Mo(VI). The successful grafting of phosphoryl groups (as tributyl phosphate derivative) is characterized by FTIR and XPS analysis, elemental analysis, titration (pH_{PZC}), TGA, BET and SEM-EDX analyses. The multi-functional characteristics of the sorbent (i.e., carboxylic, hydroxyl, amine and phosphate groups) contribute in the binding of metal ions having different physicochemical behaviors. The sorption of Nd(III) is strongly increased by phosphorylation, while for Mo(VI) the enhancement is rather limited. Optimum sorption occurs at pH 3–4: maximum sorption capacity reaches up to 1.46 mmol Nd(III) g^{-1} and 2.09 mmol Mo(VI) g^{-1}; sorption isotherms are fitted by the Langmuir equation. The equilibrium is reached within 30–40 min and the kinetic profiles are simulated by the pseudo-first order rate equation. The coefficients of the effective diffusivity are close to the self-diffusivity of Nd(III) and Mo(VI) in water; as a confirmation of the limited impact of resistance to intraparticle diffusion in the kinetic control. The sorbent is selective for Nd(III) over Mo(VI) and other alkali-earth or base metals (at pH close to 2.5–3). Metals can be readily desorbed using 0.2 M HCl/0.5 M $CaCl_2$ as the eluent. The loss in sorption does not exceed 5% at the fifth cycle, while desorption remains complete. A series of treatments (including acidic leachate, cementation, precipitation, sorption and elution) is successfully applied for the recovery of rare earths from Egyptian ore; with enrichment in the oxalate precipitate of Nd(III), Gd(III), Sm(III) and Eu(III).

Keywords:
Algal-PEI beads
Phosphorylation
Nd(III) and Mo(VI) sorption
Uptake kinetics and sorption isotherms
Metal desorption and sorbent recycling
Treatment of ore acidic leachate

1. Introduction

The development of High-Tech devices is strongly increasing the demand for rare earth elements (REEs). Incentive politics have been published in many countries and international institutions for developing the recycling of WEEE (waste electric and electronic equipment) [1,2]. An alternative source for REEs may consist of the valorization of sub-products from mineral primary resources (or secondary resources as under-marginal ores). Leaching processes are frequently used for recovering metal ions from ores and wastes; consisting in bioleaching or chemical leaching (either alkaline or acidic). In most cases, acidic leaching is preferred generating multi-component solutions that require extensive separation of valuable metals (as minor elements) from heavy metals (as major elements). This purpose generally requires combining different steps including pre-treatment such as precipitation of some major elements (under controlled conditions to prevent excessive co-precipitation of valuable metals), solvent extraction and sorption processes. Solvent extraction is highly attractive for the recovery of valuable metals at high relative concentrations [1,3]; however, environmental impact (associated with organic losses) and economic

* Corresponding author.
E-mail address: eric.guibal@mines-ales.fr (E. Guibal).

constraints may limit its application in the case of dilute effluents. Ion-exchange [4–6], chelating resins [7,8], impregnated resins [9], nano-materials [10], carbon-based sorbents [11] or metal organic framework [12] offer complementary possibilities for the recovery of valuable metals from low-concentration solutions (less than 200 mg L^{-1}). Alternative materials proceeding from natural sources (biopolymers, biomass) have been used directly for the recovery of valuable metals [13,14 15,16] or after functionalization [17].

Phosphorus-based compounds have high affinity for metal ions (including molybdate and REEs). Therefore, many extractants have been tested for liquid–liquid extraction. These attractive properties have also inspired the development of new resins bearing phosphate, phosphonate groups and so on. A new generation of resins has been recently developed based on the functionalization of algal/alginate/polyethylenimine (PEI) beads. The *in situ* partial extraction of alginate from algal biomass (eventually completed by external addition of alginate) offers the possibility to structure sorbent beads by interaction with branched PEI (bPEI) under controlled pH conditions. A complementary step of glutaraldehyde crosslinking with primary amine groups of PEI contributes to strengthen the bio-based sorbent beads (APEI). Several functional groups have been grafted onto APEI-based beads: amidoxime groups for Sr(II) sorption [18], quaternary ammonium groups (Q-APEI) for As(V) and U(VI) sorption [19,20], sulfonic groups (S-APEI) for the recovery of REEs [21]. The affinity of TBP (tributyl phosphate) for metal ions motivated the challenge of grafting TBP on APEI material. Tributylphosphate (TBP) is an extractant that was widely used for the recovery of uranyl [22], molybdenum [23–26] and rare earth [27–29] from acidic solutions. The immobilization of TBP in synthetic resin by coating [30] or embedment [31] allows extending the application of the extractant from liquid-liquid extraction (LLE) to solid/liquid separation as extractant impregnated resins (supported liquid–liquid extraction systems, SLE) and liquid–solid extractants (SPE) [32]. This efficiency for extracting target metals motivated the strategy of immobilizing TBP on alginate/PEI beads. The present study explores the grafting of TBP through a chemical functionalization of the extractant [33], before processing its immobilization on the beads to prepare P-APEI beads (phosphorylated APEI beads), using a crosslinker.

The present study focuses on the recovery of Nd(III), as a major representative of REEs, and Mo(VI) as one of associated elements in the Southwestern Sinai mining area (Egypt). The sorbent is first physically and chemically characterized using SEM and SEM-EDX, BET, TGA, elemental analyses, FTIR, XPS spectroscopies and titration (pH_{PZC}). In the second part of the manuscript, the sorption properties of P-APEI beads are investigated through the study of pH effect, uptake kinetics, sorption isotherms, selectivity, metal desorption and sorbent recycling. Finally, the sorbent is applied to the recovery of REEs and Mo(VI) from leachates produced from ores collected in Sinai (Egypt). The sorbent appears high affinity toward REEs over associated which reflects on the pure REEs oxalate cake.

2. Materials and methods

2.1. Materials

Poly(ethylene glycol) diglycidyl ether (PEGDGE) was used as a crosslinking agent; it was supplied by Shanghai Makclin Biochemical Co., Ltd. (Shanghai, China). Tributyl phosphate (TBP, $C_{12}H_{27}O_4P$) and zinc oxide were purchased from Aladdin Industrial Corporation, (Shanghai, China). Absolute ethanol, sodium hydroxide, and aluminum sulfate octadecahydrate were supplied by Guangdong Guanghua Sci-Tech Co. (Guangzhou, China). Phosphoric acid was purchased from Xilong Scientific Co., (Guangdong, China). Sulfuric acid, acetone, and toluene were supplied by Chron Chemicals (Qionglai, China). Neodymium sulfate pentahydrate was provided by National Engineering Research Centre of Rare Earth Metallurgy and Functional Materials Co., Ltd (Baotou, China). Molybdic acid ($MoO_3{\cdot}H_2O$) was used as the source of Mo(VI), which was purchased from Tianjin Guangfu Fine Chemical Research Institute (Tianjin, China). Silicon standard solution (1000 ppm) was supplied by Guobiao (Beijing, China). Branched polyethyleneimine (PEI, 50% w/w) and glutaraldehyde (GA, 50% w/w) were provided by Sigma-Aldrich (Taufkirchen, Germany). Algal biomass (*Laminaria digitata*) was obtained from Setalg, (Pleubian, France), while alginate was purchased from FMC BioPolymer (Cork, Ireland; now JRS Rettenmaier, Rosenberg, Germany). All other reagents are Prolabo products, which were used as received.

2.2. Synthesis of sorbent (Scheme 1)

2.2.1. Synthesis of algal/alginate/PEI beads (APEI)

The algal/alginate/PEI beads were prepared according a method previously described by Wang et al. [34]. The method consists of the partial extraction of alginate from algal biomass (18.75 g) using Na_2CO_3 solution (750 mL, 1% w/w) under agitation for 24 h at 50 °C. In a second step, after cooling, the suspension was completed by adding 250 mL of alginate solution (4%, w/w) to biomass suspension. Ten milliliters of PEI solution (50%, w/w) were then added to the mixture under agitation. The algal biomass/alginate/ PEI suspension was distributed dropwise through a thin nozzle into an ionotropic gelation and crosslinking batch (2 L) containing $CaCl_2$ (1%, w/w) and GA (10 mL, 50%, w/w). The beads (APEI, herein Compound A) were maintained under agitation overnight in the crosslinking solution before being filtrated, rinsed with tap water, and freeze-dried. The bead size was 2.9 ± 0.1 mm.

2.2.2. Phosphorylation of APEI beads (P-APEI)

Tributyl phosphate was first modified by reacting 68 g of TBP with 25.2 g of phosphoric acid under stirring and reflux (80 °C) for 1 h. In a second step, 23.9 g of epichlorohydrin was added dropwise to the mixture under slow agitation at 90 °C for 4 h, to produce dibutyl-(3-chloro-2-hydroxy)-propyl phosphate (Compound B).

The phosphorylation of APEI beads was performed by reaction of APEI (Compd. A, 4 g) with the mixture of Compd. B (diluted with 80 mL toluene) with 3 mL of PEGDGE (crosslinking agent). The reaction took place under agitation at 70 °C for 12 h to produce P-APEI beads. After careful washing to remove unreacted reagents, the beads were freeze-dried. The average diameter of P-APEI beads was 2.8 ± 0.1 mm.

2.3. Characterization methods

A Vario EL cube element analyzer (Elementar Analysensysteme GmbH, Langenselbold, Germany) was used for the elemental analysis of APEI and P-APEI beads. An IRTracer-100 (Shimadzu, Tokyo, Japan) was processed for collecting FTIR spectra on dried samples (conditioned into KBr discs). XPS analyses were operated using an ESCALAB 250XI + instrument (Thermo Fischer Scientific, Inc., Waltham, MA, USA). The pH-drift method was carried out for determining the pH_{PZC} of the sorbent. The sorbent (100 mg) was mixed for 48 h with 50 mL of a series of 0.1 M NaCl solutions whose initial pH values (pH_0) were controlled between 1 and 11. The final pH (pH_{eq}) was determined using a Mettler Toledo pH-meter (Mettler, Colombus, OH, USA). The pH_{PZC} is obtained for unchanged pH ($pH_0 = pH_{eq}$). Thermogravimetric analyses (TGA) were performed using a Netzsch STA 449 F3 Jupiter (NETZSCH-Gerätebau GmbH, Selb, Germany) (temperature ramp: 10 °C/min, under oxygen and/or air atmosphere). Morphological characterization and semi-quantitative surface analyses were performed on a Phenom ProX scanning electron microscope (SEM, Thermo Fisher Scientific, Netherlands) with integrated EDX facilities. Textural analysis of APEI and P-APEI materials was processed on a Micromeritics TriStar II (Norcross, GA, USA); the BJH method was used for the evaluation of both specific surface area and pore size distribution (samples were degassed at 100 °C for 12 h before analysis).

2.4. Sorption and desorption tests

Sorption and desorption experiments were carried out using the batch method. A given amount of sorbent (m, g) was mixed with a fixed volume of solution (V, L) containing the target metals (C_0: mmol L^{-1}) at room temperature (T: 21 ± 1 °C) under agitation (speed: 170 rpm). The precise experimental conditions are reported in the caption of the figures. For the pH study, the sorbent dosage (SD, m/V, g L^{-1}) was set to 1 g L^{-1}, the initial metal concentration was 0.318 mmol Nd L^{-1} or 0.632 mmol Mo L^{-1}; the contact time was set at 48 h. For uptake kinetics, the SD was 0.21 g L^{-1} for APEI and 0.3 g L^{-1} for P-APEI, the initial pH was set to 5 and the metal concentrations were: 0.318 mmol Nd L^{-1} or 0.632 mmol Mo L^{-1}. The sorption isotherms were obtained at $pH_0 = 5$, with a SD = 0.4 g L^{-1}; C_0 varied 0.069 and 3.53 mmol Nd L^{-1} and between 0.105 and 5.32 mmol Mo L^{-1}; the contact time was set to 48 h. After required contact time (intermediary times for uptake kinetics, equilibrium time: 48 h for other experiments), samples were collected, filtrated on filter membrane and the residual concentration (C_{eq}, or C(t)) was analyzed using an ICP-AES (inductively coupled plasma atomic emission spectrometer, ICPS-7510 Shimadzu, Kyoto, Japan). The mass balance equation was used for calculating the sorption capacity (q_{eq}, mmol g^{-1}); $q_{eq} = (C_0\text{-}C_{eq}) \times V/m$. Sorption in multi-component solutions followed the same experimental procedure.

Experimental conditions (especially sorbent dosage) have been adjusted between the different investigations (depending on metal and sorbent for pH study, uptake kinetics and sorption isotherms) in order to highlight the effect of target criterion. Sorbent dosage for pH study was adjusted to prevent complete metal removal to identify extensive effects of the pH. The sorbent dosages were varied for uptake kinetics to identify the contribution of resistance to intraparticle diffusion. An intermediary sorbent dosage was selected for adjusting a large concentration for metal to get a clear illustration of metal distribution between the two phases on a wide range of residual metal concentrations (and reach sorbent saturation).

For desorption tests, the metal-loaded samples collected from uptake kinetics were used for evaluating the desorption kinetics using 0.2 M HCl/0.5 M $CaCl_2$ solution as the eluent. The sorbent dosage was set to 0.8 g L^{-1}. A rinsing step was operated between each sorption and desorption step for the study of sorbent recycling. The comparison of the amounts of metal sorbed and desorbed at each step allowed calculating the efficiency of desorption. Similar procedures were used for the comparison of sorption properties of APEI and P-APEI with the performances of commercial resins (Dowex 50X8 and Dowex HCR S/S, Annex A).

2.5. Ore leaching and metal recovery

Annex B reports the leaching conditions for metal recovery from real ores and the effect of pre-treatments of these leachates on the composition of the solutions used (PPLS) for sorption tests.

2.5.1. Sorption test

The PPLS was separated into 5 fractions for testing the effect of pH on the recovery and separation of target metal ions. Initial pH values were set to 1.02, 2.02, 3.06, 4.01 and 5.01 using 0.1 M NaOH and H_2SO_4 solutions. The sorbent was added to the PPLS solution at a sorbent dosage of 0.5 g L^{-1}. After 48 h of agitation (v: 170 rpm), the solution was filtrated and the residual concentration for selected metals was analyzed by ICP (or spectrophotometry for the global index of REEs, [35]).

2.5.2. Eluate treatment and REE recovery

Loaded sorbent was eluted with 0.2 M HCl/0.5 M $CaCl_2$ solution. Oxalate being a selective precipitant for REEs, the eluate was treated with a 25% (w/w) oxalic acid solution at pH 1.1 and room temperature for 45 min. A white precipitate was formed which recovered by filtration. EDX analysis was performed for characterizing the precipitate.

3. Results and discussion

3.1. Sorbent characterization

3.1.1. Morphological and textural characteristics

Fig. S1 shows SEM micrographs of APEI and P-APEI sorbents associated with the semi-quantitative EDX analysis of their surfaces and crosscut sections. The beads are characterized by a pleated surface due to the shrinking of the hydrogel beads during the final drying step. Apparently, APEI shows more pores on the surface. After cross-cutting, the highly porous structure of the beads appears; the thin scaffolds (less than 5 μm) show very smoothed surfaces forming interconnected internal pores as large as 100–150 μm. The structure of the beads allows anticipating that the resistance to intraparticle diffusion will have a very limited impact on mass transfer; the main resistance to diffusion will occur through the outer "skin" of the beads. The semi-quantitative analysis of the beads shows that the sorbents are roughly homogeneous: the atomic percentages are of the same order of magnitude while comparing the elemental distribution at the surface and in the cross-cut section. For APEI, the main difference concerns the lower N fraction in the core of the beads compared with external surface. Consistently with the synthesis of the beads, APEI shows a high content of nitrogen (9.36–12.74%, atomic; 5.8–7.21%, weight), essentially brought by PEI. The efficient phosphorylation is confirmed by the relative increase of O content and the appearance of phosphorus (5.17–5.45%, atomic; 6.84–7.07%, weight). Because of the grafting of TBP-derivative, the relative fraction of N in P-APEI slightly decreases. It is noteworthy that Cl content also decreases after functionalization of APEI beads: the residues of $CaCl_2$ (used for ionotropic gelation of alginate) are probably washed up during chemical modification.

Fig. S2 provides the textural characteristics of APEI and P-APEI beads. The isotherms of nitrogen sorption and desorption show marked hysteresis between the sorption and the desorption branches, which is usually associated with Type IV isotherm in the IUPAC classification (Fig. S2a) [36]. This shape is also frequently associated with mesoporous materials. It is consistent with the pore size distribution appearing in Fig. S2b: (a) significant shifts in the widths of the pores when comparing the sorption and desorption curves and (b) order of magnitude of the average pore size (below 50 nm, though some pores may reach up to 110 nm). The structuration of the raw beads results from the combined effects of alginate ionotropic gelation (with calcium cations) and glutaraldehyde crosslinking of PEI (through primary amine groups of the polymer chain and aldehyde groups of GA). The final porosity is also controlled by the drying procedure. Valentin et al. [37] reported the dramatic influence of drying procedure on alginate gel porosity: BET specific surface area decreased from 300-400 $m^2\ g^{-1}$ for aerogels (dried under supercritical CO_2 conditions) to a few $m^2\ g^{-1}$ for xerogels (air-drying). Freeze-drying of alginate gels offers intermediary values for specific surface area (from 10 to 250 $m^2\ g^{-1}$) [38]. The phosphorylation of APEI beads leads to a weak decrease in the specific surface area (from 44.3 to 24.7 $m^2\ g^{-1}$), while the porous volume is halved (from 0.265 to 0.123 $cm^3\ g^{-1}$). The complementary chemical modifications (passing through solvent systems), the new linkages and the supplementary freeze-drying step may explain this decrease. The large size of the pores may be correlated with the weak porous volume and limited specific surface area. This means also that the diffusion of metal ions will not be significantly hindered by the porosity of the sorbent.

It is thus possible anticipating that the accessibility to reactive groups is not controlling the mass transfer properties and that the uptake kinetics will be fast (see Section 3.2.2).

3.1.2. Thermogravimetric analysis

Fig. S3 compares the thermal degradation profiles for APEI and P-APEI beads (under oxidative atmosphere, O_2). Different phases can be identified. In the range 0–150 °C (for P-APEI) or 0–200 °C (for APEI), the materials lose absorbed water. It is noteworthy that the amount lost is

much smaller for P-APEI (i.e., less than 3%) than for APEI (9.6%). The DTG curves show local minima at 120.1 °C for P-APEI and 137.8 °C for APEI.

In the range 150 °C (or 200 °C) to 320–350 °C, the two degradation curves are almost overlapped, with the decomposition of a first group of compounds probably associated with the APEI structure (i.e., depolymerization of PEI, degradation of carboxylic groups of alginate, etc.). The DTG curve for APEI shows a small valley at 230.66 °C, and more marked extremum at 348.26 °C (at 314.49 °C for P-APEI). Weight loss reaches around 40%.

Above 350 °C, the curves diverge for the two sorbents. For APEI, the weight loss continues almost linearly up to 650 °C. Actually, two sections with different slopes can be reported and correlated to the valleys observed on DTG curves at 348.26 °C, 503.26 °C, and 555.06 °C. The oxidative degradations of alginate and PEI compounds continue and represent about 90%; a valley is identified at 555.06 °C (inflexion point of the TGA curve). In the case of P-APEI, the weight loss is shifted toward higher temperatures with two sequences: (a) up to ~550 °C, and (b) up to ~800 °C. These evolutions can be correlated with two valleys at 487.69 °C and 740.29 °C. The weight loss, stabilized at about 800 °C, represents 85%. The general shape of P-APEI thermal degradation is consistent with the profile obtained on TBP-grafted silica (under nitrogen atmosphere) [33]. The phosphorylation of APEI beads slightly improves the thermal stability of the material. The incorporation of phosphorus–based compounds is a well-known process for improving the fire-retardant properties of materials [39].

3.1.3. *FTIR spectroscopy*

FTIR spectroscopy is a useful tool for characterizing the chemical modification of the sorbent. The phosphorylation of APEI is confirmed by the strong changes in the FTIR spectrum (Fig. 1 and Fig. S4). The most relevant changes concern (Tables S2a and S2b):

(a) The increase in the intensity of the C—H bands in the region 3000–2800 cm^{-1}; this is directly correlated to the butyl groups brought by TBP grafting.

(b) The appearance of a peak at 1739 cm^{-1}; which is associated to the stretching ester vibration (C(═O)O) overlapped with carboxylate groups of alginate.

(c) The appearance of the C—H bending band at 1465 cm^{-1}.

(d) The appearance of the P═O peak (asymmetric stretching) at 1257 cm^{-1}.

(e) The strong increase in the intensity of the band at 10321 cm^{-1} (corresponding to contributions of C—C, C—O stretching vibrations and –OH out-of-plane bending vibration).

(f) The appearance of small peaks at 507, 594 and 812 cm^{-1} (associated with P-O-C stretching vibrations).

It is noteworthy that amine groups supposed to appear close to 1594 cm^{-1} in branched PEI almost disappear, being replaced with amide groups [40], whose stretching vibration appears at 1635 cm^{-1}. This is important since the (non-protonated) amine groups can bind metal cations through chelation in near neutral solutions while their protonation (or the protonation of amide groups) in acidic solutions allows binding metal anions.

The interactions of the sorbents with metal ions can be also identified through the changes in the FTIR spectra of these materials: the involvement of the reactive groups (or at least the modification of their environment) may induce shifts; appearance/disappearance of specific bands on the spectra (Fig. 1 and Fig. S4b). In the case of Mo(VI) and Nd (III) sorption onto APEI beads, the main differences are marked by:

(a) The decrease of the relative intensity of the peak at 1382 cm^{-1} (i.e., symmetric stretching of C—O in carboxylate).

(b) The shift of the peak at 1096 cm^{-1} to 1119 cm^{-1} for Mo(VI) or 1117 cm^{-1} for Nd(III); it is noteworthy that after desorption and five recycling steps, the peak remains shifted in the range 1115–1117 cm^{-1}. This peak may be assigned to C—O—C and C—O stretching; this means that the chemical environment of these functional groups is affected by metal binding.

(c) The appearance of a peak at 617–619 cm^{-1}, which does not disappears after metal desorption. This was attributed to sulfate binding (directly on protonated amine groups and/or through the binding of metal sulfate complexes, especially for Nd(III)).

The changes are much more marked in the case of P-APEI sorbent; the higher sorption levels facilitate the identification of spectral changes (Table S2b). The sorption of Mo(VI) and Nd(III) is followed by the decrease in the relative intensity of the peak at 1739 cm^{-1} (assigned to C(═O)O ester stretching vibration). It is noteworthy that the band is restored after metal desorption (after 5 cycles). A new band is appearing at 1416 cm^{-1} after the sorption of both Mo(VI) and Nd(III), which disappears after metal desorption. The band at 619 cm^{-1} that was already reported for APEI sorbent is also observed for P-APEI (assigned to sulfate, with higher relative intensity). However, the most representative changes are observed in the regions corresponding to phosphate specific vibrations:

(a) The band at 1257 cm^{-1} (asymmetric P═O stretching) almost

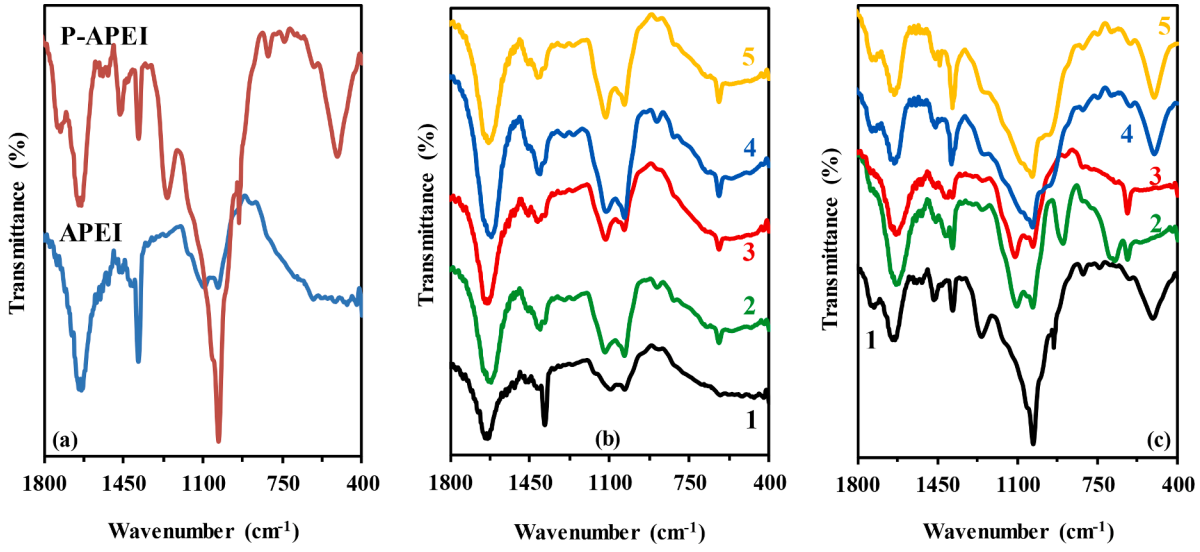

Fig. 1. FTIR spectra of raw materials (a) and APEI (b) and P-APEI sorbent (c) (before (1) and after metal sorption (2: Mo, 3: Nd) and metal desorption (4: Mo, 5: Nd)) – Focus on 1800–400 cm^{-1} wavenumber range.

disappears with the sorption of either Mo(VI) or Nd(III); the band is only partially restored after metal desorption.

(b) The band at 507 cm^{-1} (P-O-C stretching) disappears with metal bind but this vibration fully re-appears after metal desorption.

(c) A new strong band appears at 1101 cm^{-1} for both Mo(VI) and Nd (III) –loaded sorbents. This may be associated with phosphate interaction (P-O bond) with metal ions.

(d) The sorption of Mo(VI) shows specific and strong new bands at 899, 687 and 671 cm^{-1}, which disappear after metal desorption. Sen et al. [41] reported an analytical FTIR band at 911 cm^{-1}. Sadighi et al. [42] reported Mo-O stretching at 620 cm^{-1} and Mo-O-Mo stretching and bending vibrations at 880 and 990 cm^{-1}, respectively. Since the 899 cm^{-1} band can be assigned to Mo-O-Mo stretching, it is possible suggesting that polynuclear molybdate species are bound. Fig. 1b shows that the peak appearing at 1118 cm^{-1} (for Mo(VI) uptake) and 1113 cm^{-1} (for Nd(III) binding) are markers of metal binding for APEI; in the case of P-APEI, this peak appears at 1101 cm^{-1} and 1107 cm^{-1}, respectively. It is noteworthy that in the case of APEI after metal desorption, this new peak is maintained contrary to the case of P-APEI, where the spectra were restored (the spectra were closer to those of initial materials). In the case of APEI, the peak at 1095 cm^{-1}, assigned to C—O—C and C—O stretching, is shifted toward higher wavenumber after the sorption of both Mo(VI) and Nd(III). Despite metal desorption, this shift is maintained indicating that the environment of C-O groups is durably affected by sorption (metal binding) and desorption (ion-exchange with calcium contained in the eluent for stabilization of carboxylate groups) steps. On the other side, in the case of P-APEI, the presence of phosphoryl groups contributes to the strong binding of metal ions (preferentially to carboxylic and carbonyl groups, which are affected by phosphoryl grafting). The peak appearing at ~1030 cm^{-1} (and/or other wavelets marked by weak shoulders at ~ 1050 cm^{-1}) is shifted or increased (in relative intensity) after metal binding. This is a confirmation that phosphoryl-based groups are involved in metal binding for P-APEI. Metal desorption is followed by the disappearance of this peak that confirms the reversibility of metal binding.

Appearing usually around 932 cm^{-1} [43], or 962–963 cm^{-1} [44,45] in phosphomolybdate-based compounds and composites, in the present case M═O stretching is observed at ~901 cm^{-1} after molybdate sorption onto P-APEI.

In the case of APEI sorbent, the bands associated with carbonyl and/or carboxyl groups appear to be the most affected by metal binding, as an evidence of chelation or ion-exchange on carboxylate groups. On the opposite hand, in the case of P-APEI sorbent, the most significant changes affect phosphate-based reactive groups. It is noteworthy that FTIR spectroscopy does not allow identifying substantial changes to amine groups (from PEI) due to the modification of their chemical environment during chemical modification (this is confirmed by XPS characterization), which limits their chelation affinity and/or their availability and accessibility for ion-exchange.

3.1.4. *XPS spectroscopy*

The comparison of the XPS survey curves (Fig. 2) for APEI and P-APEI materials clearly confirms the successful immobilization of phosphonate groups onto the support with the appearance of two peaks at binding energies (BE) around 133 eV and 190 eV corresponding to P 2p and P 2 s signals, respectively. It is noteworthy that the weak peak at 349 eV associated with Ca 2p signal disappears after functionalization, while the relative intensities of S 2p (at 167 eV) and S 2s (at 198 eV) slightly decrease. The N 1s signal at 399 eV is also significantly reduced: the grafting of chemically-modified TBP affects the environment of N groups.

The sorption of Nd(III) onto P-APEI is shown by the appearance of a series of typical peaks at 121 eV (Nd 4d), 230 eV (Nd $4p_{3/2}$) and 246 eV (Nd $4p_{1/2}$). The peaks corresponding to Nd $3d_{5/2}$ (984 eV) and Nd $3d_{3/2}$ (1004 eV) are partially superposed with the O KL1 (981 eV) and O KL2 (1000 eV) signals making difficult their identification on the survey XPS

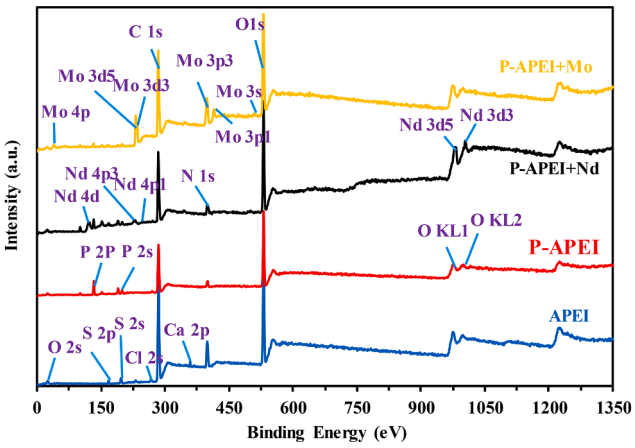

Fig. 2. XPS spectra (survey) for APEI and P-APEI beads (for functionalized sorbent, spectra are compared before and after Mo(VI) and Nd(III) sorption).

curve. In the case of Mo(VI)-loaded sorbent, the signals at 40 eV (Mo 4p), 231 eV (Mo 3d), 399 eV (Mo $3p_{3/2}$, superimposed with N 1s signal), 415 eV (Mo $3p_{1/2}$) and 502 eV (Mo 3s) confirm the binding of molybdate anions onto the sorbent.

The comparison of high-resolution XPS spectra (HRES) for C 1s, O 1s, N 1s shows substantial changes associated with the grafting of TBP derivative (i.e., dibutyl-(3-chloro-2-hydroxy)-propyl phosphate, DBCHPP) with polyethylene glycol diglycidyl ether (PEGDGE, as the crosslinking agent) on APEI (Fig. S5a and S5b). The most significant changes are observed on C 1s signal with the increase in the relative intensity (atomic fraction) of C═C bond and the enlargement of the signal (FWHM) due to the formation of supplementary bonds (for example C-O-P). The O 1s appears more symmetrical after phosphorylation due to the contribution of P═O bonds that counterbalances the contribution of C═O in the raw material. Although the general shape of the N 1s spectrum is hardly affected by phosphorylation, the contribution of the peak representing $N_{tert.}$ is apparently increased due to the modification of the environment of N groups while grafting DBCHPP through PEGDGE crosslinking. Obviously, the immobilization of TBP derivative allows the appearance of P 2p signal, which can be deconvoluted into two signals corresponding to P-O-C (at BE: 132.75 eV, about 90 % AF) and phosphate bonds (at BE: 134.0 eV, about 10% AF).

The binding of Nd(III) and Mo(VI) induces some changes to the C 1s signal: the relative intensities of the 2 main contributions corresponding to C═C and C-(H,C,N,O) bonds are reversed after metal binding. In addition, the "tailing" of the spectrum (corresponding to C-═O, C-O(-C, P) shows a larger contribution and the reinforcement of C—O and C═N bonds. The environment of N and P reactive groups is influenced by the binding of both Nd(III) and Mo(VI). Substantial differences are observed in the case of O 1s signal between Nd(III) and Mo(VI). Indeed, the binding of molybdate (oxoanion) substantially increases the proportion of oxygen on the material: the FWHM drastically increases after molybdate binding as shown in Table S3. The N 1s spectrum is also significantly changed by the sorption of Nd(III): the $N_{tert.}$ band is shifted toward higher BE and completed by the appearance of a π-π* satellite signal. This satellite signal is not appearing in the case of Mo(VI) sorption. On the opposite hand, the contribution of N_{tert} bond decreases while the FWHM of N 1s signal is strongly increased. The binding of molybdate involves much stronger changes on the environment of nitrogen-based reactive groups. The observation of the spectra for the P 2p signal shows that in the case of Nd(III) uptake, the symmetrical shape of the peak with contributions of P-O-C and phosphate groups is roughly maintained (with a little decrease in the contribution of phosphate group). The binding of the metal ions is also confirmed by the Nd $3d_{5/2}$ and Nd 4d (poorly resolved) signals; the deconvolution of Nd $3d_{5/2}$ signal in two peaks means that Nd(III) is present under two different

forms, probably associated with different binding modes of interaction or different functional groups. The analysis of Mo 3d and Mo 3p signals also allows identifying two peaks corresponding to heterogeneities in the mode of interaction or the reactive groups involved in metal binding.

Contrary to FTIR spectroscopy, XPS analysis shows that the binding of both Nd(III) and Mo(VI) changes the chemical environment of both N and P elements. However, the sorption of Mo(VI) shows a stronger impact on the N-based reactive groups compared with Nd(III): this is due to the binding of molybdate anionic species on protonated amine groups. The contribution of amine groups in terms of Nd(III) chelation is considerably lower. For Mo(VI), sorption mainly occurs through both the interaction of the metal anions with protonated amine groups and the formation of phosphomolybdate species, while for Nd(III), most of binding occurs through the interaction of the metal cation with phosphate-based reactive groups.

3.1.5. Elemental analysis and pH_{PZC}

Table 1 shows the elemental analysis of the two materials; the successful phosphorylation of APEI is demonstrated by the presence of phosphorus in the functionalized sorbent. TBP grafting is associated with a mass fraction of phosphorus close to 5.15% representing a molar content of 1.66 mmol P g^{-1}. Following TBP grafting, the molar content of amine groups decreases from 4.18 to 3.1 mmol N g^{-1}. This means that the N/P molar ratio is close to 1.87. In branched PEI, the distribution of primary, secondary and tertiary amine groups is 1:2:1. After glutaraldehyde cross-linking (which preferentially operates on primary amine groups), the relative fraction of primary amine groups is even reduced. The stoichiometric ratio N/P means that the phosphorylation operates not only on primary but also probably on secondary or tertiary amine groups. The presence of S element in APEI beads is probably associated with amino groups and fucoidan from algal biomass. After phosphorylation, the contribution of S is drastically reduced (almost undetectable). Among the most representative reactive groups on the sorbents it is possible anticipating the contribution of carboxylic groups (of alginate from algal biomass and associated amino-acids and proteins), and the amine groups (mainly from PEI, but also with weak contributions of proteins from the algal biomass) for APEI. In the case of P-APEI, phosphate reactive groups may also contribute to the global multi-functional reactivity of the sorbent.

Several methods can be used for analyzing surface charge of the sorbent and determining the pH_{PZC} of the materials. Although zetametry is frequently used, the pH-drift method was also very often used for getting the pH-frontier between positive charged and neutral (or negatively charged) surface [46]. Some discrepancies may be observed, but generally the values are close enough to help in understanding the effect of pH on metal sorption. Fig. S6 compares the pH_{PZC} values (obtained by the pH-drift method) for APEI and phosphorylated APEI. The successful functionalization is confirmed by the drastic decrease in the pH_{PZC} value from 6.54 for APEI to 2.75 for P-APEI. Apart highlighting the chemical modification of the support, this information shows that the sorbent is deprotonated on a wider range of pH compared with the raw material. This means that the affinity of the APEI sorbent for anionic species (ion-exchange and electrostatic attraction) will be extended on a larger pH range while the repulsion of cationic species will be also active at much higher pH values. On the opposite hand, for P-APEI, the positive charge of the sorbent (favorable to the binding of molybdate anionic species) will operate on a shorter range of pH, while the repulsion of metal cations will be decreased at intermediary pH values (around 3). This is critical for designing and optimizing the sorption process. For example, Zeng et al. [47] synthesized a series of phosphonate-functionalized polystyrene resins and tested their sorption properties for U(VI). They observed the strong effect of the zeta potentials (ZPs) of the different resins (negative, neutral and positive ZPs) on both the sorption capacities but also the type of bound species (in relation with metal speciation) [47]. These acid-base properties allow also anticipating a more important pH change during the sorption process (i.e., pH decrease with proton capture).

3.2. Sorption properties

3.2.1. pH effect

Fig. 3 shows the effect of equilibrium pH on the sorption of Nd(III) and Mo(VI) for both APEI and P-APEI sorbents. Initial pH was systematically varied between 1 and 6. While for APEI the pH hardly changes during metal sorption (Fig. S7), the pH strongly decreased above pH_0 3; these trends are consistent with the amplitude of pH variation appearing in Fig. S8 (pH-drift method applied for determination of pH_{PZC}). Therefore, in the case of P-APEI, the effect of equilibrium pH is only followed between 1 and 3.5–4 for Nd(III) to prevent metal precipitation

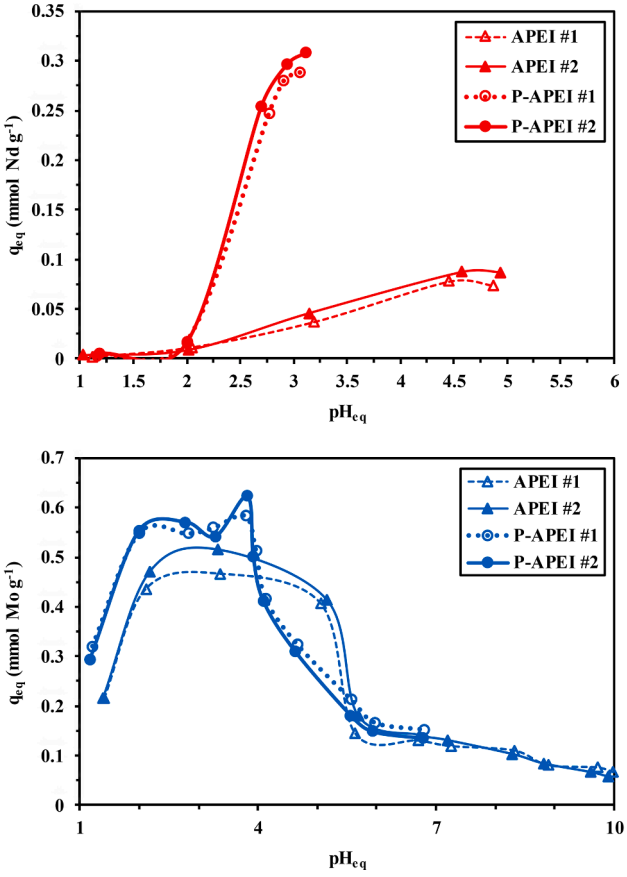

Fig. 3. Effect of pH on Nd(III) and Mo(VI) sorption capacity using APEI and P-APEI sorbents (C_0: 0.31 mmol Nd L^{-1} or 0.61 mmol Mo L^{-1}; Sorbent dosage, SD: 1 g L^{-1}; Time: 48 h; Agitation: 210 rpm; T: 22 ± 1 °C).

Table 1
Elemental analysis of raw beads (APEI) and phosphorylated beads (P-APEI).

Sorbent	C (%)	H (%)	O (%)	S (%)	S (mmol g^{-1})	N (%)	N (mmol g^{-1})	P (%)	P (mmol g^{-1})
APEI beads	39.43	6.98	35.01	0.41	0.13	5.85	4.18	n.d.	–
P-APEI beads	41.05	8.4	40.98	0.03	0.01	4.34	3.10	5.15	1.66

n.d.: not detectable.

at pH_0 higher than 6. In the case of Mo(VI), the pH_0 range was extended up to pH 11: the final pH for APEI varies between 1.39 and 9.99, while for P-APEI , the pH variation ranges between 1.16 and 6.81.

In the case of Nd(III), the sorption is negligible in the range pH_{eq} 1–2 for both APEI and P-APEI beads. Neodymium is essentially present under cationic species (>87%) at pH below 3 and totally under the form of $NdSO_4^+$ and Nd^{3+} above pH 3. Above pH 2, the concentration of free Nd (III) increases up to pH 4 and stabilizes around 53% at higher pH. At pH above 3, APEI sorbent is partially protonated and can bind metal Nd(III) cations; this is the main reason for the little increase in the sorption capacity (to reach less than 0.09 mmol Nd g^{-1}). In the case of P-APEI, the sorbent remains protonated in acidic solutions. The protonation decreases with increasing the pH, the competition effect of protons progressively decreases and the sorption capacity strongly increases: at pH_{eq} 3 (corresponding to pH_0: 4–5), the sorption capacity reaches 0.29 mmol Nd g^{-1}; i.e., more than 6 times the sorption capacity obtained with APEI. The phosphorylation of APEI strongly enhances Nd(III) sorption through the interaction of Nd(III) with phosphate groups and amine groups (consistently with FTIR and XPS characterizations). This sorption is enhanced by the progressive deprotonation of the reactive groups. In the case of molybdate, the sorption capacities are slightly higher and the phosphorylation hardly changes the sorption capacities (under selected experimental conditions): the curves for APEI and P-APEI are almost superposed. In acidic solutions (pH 1–1.5) the sorption capacity is close to 0.2–0.3 mmol Mo g^{-1}, while the pH increases the sorption capacity increases up to a plateau close to 0.45–0.5 mmol Mo g^{-1} for APEI, and 0.5–0.6 mmol Mo g^{-1} for P-APEI in the range pH_{eq} 2–4. Above pH_{eq} 4, the sorption capacity sharply decreases down to 0.07 mmol Mo g^{-1} for APEI and 0.14 mmol Mo g^{-1} for P-APEI. The profile is consistent with the speciation diagram of molybdate that shows the predominance of neutral molybdate species in acidic solutions (i.e., pH < 3.5), the appearance of polynuclear anionic species ($H_3Mo_8O_{28}^{5-}$, $H_2Mo_7O_{24}^{5-}$ and $H_2Mo_6O_{21}^{4-}$) together with $HMoO_4^-$ in the intermediary pH range (i.e., pH 2–6), and the predominance of MoO_4^{2-} at pH > 4.3. The maximum sorption is correlated to the presence of polynuclear polyhydrolyzed species while the predominance of neutral (low pH) or di-anionic mononuclear species (close to neutral) reveals unfavorable. Protonated amine groups readily bind molybdate anionic species (preferentially polynuclear as previously shown for chitosan-based sorbents, [48]); while increasing the pH, the deprotonation reduces the ability of these groups to bind molybdate species. The formation of phosphomolybdic species in acidic solutions is a well-known reaction that is frequently used for phosphate analysis [49]. Therefore, the sorption of molybdate species may proceed through the interactions of molybdate with phosphate groups and with protonated amine groups, under pH control (metal speciation, protonation/deprotonation of reactive groups). It is noteworthy that, at least under the experimental conditions selected for the study of pH effect (including the limitation of the equilibrium pH range for P-APEI; i.e., pH 1–3.4), the phosphorylation hardly increases the sorption capacity for Mo(VI). In addition, the superposition of the curves (runs #1 and #2) shows that the sorption properties are reproducible.

3.2.2. Uptake kinetics

Fig. 4a shows the kinetic profiles for the sorption of Nd(III) and Mo (VI) using both APEI and P-APEI at two levels of metal concentration (i.e., 50 and 500 mg L^{-1}; i.e., 0.347 and 3.47 mmol Nd L^{-1} or 0.521 and 5.21 mmol Mo L^{-1}). The replicates show again the good reproducibility of sorption performance. These results confirm the conclusions raised in the study of pH effect: the phosphorylation significantly improves the sorption capacity for Nd(III): the residual concentration is strongly reduced, while the enhancement is more gradual and less marked in the case of Mo(VI). In the case of Nd(III), it is noteworthy that the functionalization of the beads drastically reduces the equilibrium time: 20–30 min instead of 60 min for APEI beads. For Mo(VI), the uptake kinetics are apparently less affected by the chemical modification of raw

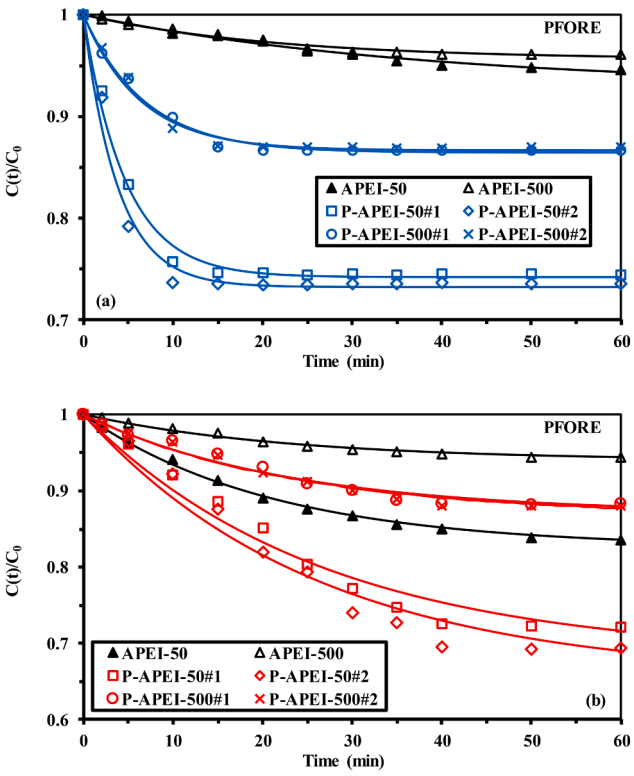

Fig. 4a. Uptake kinetics for Nd(III) (a) and Mo(VI) (b) using APEI and P-APEI beads (C_0: 50 or 500 mg mg L^{-1}; pH_0: 5, except for APEI/Mo(VI) system where pH_0 was set to 3; SD: 0.21 g L^{-1} for APEI and 0.3 g L^{-1} for P-APEI beads; T: 21 ± 1 °C; solid curves: modeling with the pseudo-first order rate equation).

beads and the mass transfer is globally slower than for Nd(III): a contact time of 60 min is systematically necessary.

The kinetic profiles have been modeled using different equations (pseudo-first order rate equation, PFORE, pseudo-second order rate equation, PSORE, and the Crank equation for resistance to intraparticle diffusion, Table S1a). Table 2a compares the determination coefficients, the calculated equilibrium sorption capacities, and the Akaike

Table 2a
Uptake kinetics for Nd(III) sorption onto APEI and P-APEI beads – Modeling with the PFORE, the PSORE and the RIDE.

Model	Sorbent	APEI		P-APEI			
	C_0 (mg L^{-1})	50	500	50 Run #1	50 Run #2	500 Run #1	500 Run #2
Exper.	q_{eq} (mmol g^{-1})	0.095	0.641	0.319	0.298	1.48	1.53
PFORE	$q_{eq,1}$ (mmol g^{-1})	0.127	0.724	0.322	0.301	1.50	1.56
	$k_1 \times 10^2$ (min^{-1})	2.61	4.64	21.2	25.9	14.5	15.7
	R^2	0.988	0.979	0.994	0.987	0.991	0.989
	AIC	−142	−143	−115	−105	−126	−123
PSORE	$q_{eq,2}$ (mmol g^{-1})	0.199	1.01	0.357	0.328	1.72	1.78
	$k_2 \times 10$ (L $mmol^{-1}$ min^{-1})	0.875	0.370	8.20	11.3	10.8	11.3
	R^2	0.986	0.970	0.966	0.952	0.971	0.962
	AIC	−140	−139	−95	−90	−111	−108
RIDE	$D_e \times 10^8$ (m^2 min^{-1})	1.85	2.70	7.64	9.26	6.03	6.44
	R^2	0.956	0.929	0.978	0.967	0.980	0.973
	AIC	−123	−92	−102	−97	−117	−113

C_0: 0.35 mmol Nd L^{-1} or 3.5 mmol Nd L^{-1}.

Information Criterion (AIC) for the different models and the different systems. The PFORE systematically reports higher determination coefficients, closer values for $q_{eq,calc}$ *vs.* $q_{eq,exp.}$ and lower AIC values compared with the other models. Fig. 4a also shows the good superposition of experimental profiles with the PFORE fitted curves.

The change in the initial concentration (i.e., 50 to 500 mg metal L^{-1}) does not significantly change the apparent rate coefficient (Table 2b). For Nd(III), k_1 varies between 2.61×10^{-2} min^{-1} and 4.64×10^{-2} min^{-1} in the case of APEI, for P-APEI the rate coefficient is slightly higher: from 21.2 to 25.9 $\times 10^{-2}$ min^{-1} at 0.35 mmol Nd L^{-1} to 14.5–15.7 $\times 10^{-2}$ min^{-1} at 3.47 mmol Nd L^{-1}. In the case of Mo(VI), the apparent rate coefficients hardly vary with metal concentration and are of the same order of magnitude for APEI (4.74–4.35 $\times 10^{-2}$ min^{-1}) and P-APEI (3.75–4.41 $\times 10^{-2}$ min^{-1}).

The kinetic profiles are not perfectly fitted by the Crank equation; therefore, the diffusivity coefficients deduced from these fits should be considered as indicative. The effective diffusivity coefficient is weakly affected by the type of sorbent and the metal concentration for Mo(VI) (Tables 2a-b): 1.58–2.27 $\times 10^{-8}$ m^2 min^{-1}. In the case of Nd(III), the effective diffusion coefficient is lower for APEI (1.85–2.70 $\times 10^{-8}$ m^2 min^{-1}) than for P-APEI (6.03–9.26 $\times 10^{-8}$ m^2 min^{-1}; D_e slightly decreases with metal concentration). The diffusivity of Nd(III) in water is close to 3.7×10^{-8} m^2 min^{-1} while that of Mo(VI) is near 1.19×10^{-7} m^2 min^{-1} [50]. This mean that Nd(III) effective diffusivity in APEI is only halved compared with its self-diffusivity in water; this means that the resistance to intraparticle diffusion has a limited impact on mass transfer. This effect is even decreased for P-APEI (despite the little decrease in porous properties, Section 3.1.1). In the case of Mo(VI), the effective diffusivity in the sorbents is about one order of magnitude lower than the self-diffusivity in water: the resistance to intraparticle diffusion plays a greater role in the control of mass transfer; this may be explained by the size of molybdate species and the formation of polynuclear species.

Table 2c reports the parameters of the kinetic models for Nd(III) and Mo(VI) removal from binary equimolar solutions (Fig. 4b). As expected, both the sorption capacity and the equilibrium times are improved while using P-APEI compared with raw material. The parameters (apparent rate coefficients k_1 and the effective diffusivities) are of the same order of magnitude than for mono-component solutions: the presence of the competitor (or co-metal) does not drastically change the mass transfer

Table 2b
Uptake kinetics for Mo(VI) sorption onto APEI and P-APEI beads – Modeling with the PFORE, the PSORE and the RIDE.

Model	Sorbent	APEI		P-APEI			
	C_0 (mg L^{-1})	50	500	50 Run #1	50 Run #2	500 Run #1	500 Run #2
Exper.	q_{eq} (mmol g^{-1})	0.461	1.42	0.539	0.519	2.10	2.15
PFORE	$q_{eq,1}$ (mmol g^{-1})	0.479	1.55	0.607	0.592	2.32	2.35
	$k_1 \times 10^2$ (min^{-1})	4.74	4.35	3.75	3.82	4.41	4.28
	R^2	0.997	0.987	0.976	0.971	0.973	0.981
	AIC	−147	−152	−101	−95	−123	−127
PSORE	$q_{eq,2}$ (mmol g^{-1})	0.616	2.05	0.829	0.809	3.05	3.11
	$k_2 \times 10^2$ (L $mmol^{-1}$ min^{-1})	7.34	1.91	3.76	3.92	1.30	1.23
	R^2	0.989	0.973	0.961	0.953	0.955	0.966
	AIC	−128	−143	−94	−90	−117	−120
RIDE	$D_e \times 10^8$ (m^2 min^{-1})	2.07	2.27	1.59	1.58	2.11	2.00
	R^2	0.984	0.966	0.945	0.937	0.946	0.957
	AIC	−119	−137	−88	−84	−113	−114

C_0: 0.55 mmol Mo L^{-1} or 5.5 mmol Mo L^{-1}.

Table 2c
Uptake kinetics for Nd(III) and Mo(VI) sorption onto APEI and P-APEI beads from binary solutions – Modeling with the PFORE, the PSORE and the RIDE.

Model	Sorbent	APEI		P-APEI	
	Metal	Nd(III)	Mo(VI)	Nd(III)	Mo(VI)
Exper.	q_{eq} (mmol g^{-1})	0.050	0.331	0.285	0.297
PFORE	$q_{eq,1}$ (mmol g^{-1})	0.054	0.384	0.291	0.327
	$k_1 \times 10^2$ (min^{-1})	5.56	2.27	14.5	4.47
	R^2	0.937	0.998	0.993	0.966
	AIC	−141	−152	−123	−110
PSORE	$q_{eq,2}$ (mmol g^{-1})	0.069	0.568	0.327	0.431
	$k_2 \times 10^2$ (L $mmol^{-1}$ min^{-1})	79.3	2.92	59.2	9.29
	R^2	0.913	0.996	0.964	0.947
	AIC	−136	−143	−103	−105
RIDE	$D_e \times 10^8$ (m^2 min^{-1})	2.96	0.39	5.42	2.07
	R^2	0.915	0.977	0.976	0.936
	AIC	−136	−115	−109	−101

Table 3
Nd(III) and Mo(VI) sorption isotherms using APEI and P-APEI beads – Modeling with Langmuir, Freundlich and Sips equations.

Sorbent		APEI		P-APEI			
Model	Metal	Nd (III)	Mo (VI)	Nd(III)		Mo(VI)	
				Run #1	Run #2	Run #1	Run #2
Exper.	q_m (mmol g^{-1})	0.605	1.46	1.47	1.45	2.10	2.08
Langmuir	$q_{m,L}$ (mmol g^{-1})	m, h	2.20	1.94	1.91	2.75	2.69
	b_L (L $mmol^{-1}$)		0.384	1.22	1.28	0.827	0.863
	R^2		0.969	0.988	0.988	0.991	0.994
	AIC		−45	−55	−56	−51	−55
Freundlich	k_F	0.87	0.640	0.985	0.985	1.16	1.15
	n	0.978	1.90	2.22	2.23	2.18	2.20
	R^2	0.905	0.988	0.978	0.966	0.978	0.981
	AIC	−4	−59	−50	−45	−42	−43
Sips	$q_{m,S}$ (mmol g^{-1})	m	m.	2.28	1.83	3.09	3.05
	b_S (L $mmol^{-1}$)			0.847	1.45	0.664	0.676
	n_s			1.22	0.927	1.16	1.17
	R^2			0.987	0.989	0.991	0.994
	AIC			−52	−52	−48	−53

m.: meaningless; h: Henry's Law: q (mmol Nd g^{-1}) = 0.1910 C_{eq} (mmol Nd L^{-1}, $R^2 = 0.997$; AIC = −96).

Table 4
Selectivity tests for metal recovery from multi-component equimolar solutions (C_0: ≈ 1 mmol metal L^{-1}) at different pH values for APEI and P-APEI sorbents – Comparison of distribution ratios for selected metals and D_{max}/D_{min} ratio.

Sorbent	pH	Ranking	D_{max}/D_{min}
APEI	1.38	**Mo** ≫ Zn ≫ Al ≈ **Nd** ≈ Si > Ca > Fe ≈ **Eu**	6.97
	2.27	Zn ≫ **Mo** ≫ **Nd** > **Eu** ≫ Al > Si > Fe > Ca	11.0
	3.53	Zn ≫ **Mo** > Fe ≫ **Nd** ≈ **Eu** > Ca > Al > Si	5.34
	4.22	Zn > Fe ≫ Ca ≫ Al ≈ **Eu** > Si ≈ **Nd** ≈ **Mo**	4.18
	5.39	Fe ≈ Zn > Ca > Al ≫ **Nd** > **Mo** > **Eu** > Si	4.59
P-APEI	1.27	**Nd** ≫ **Mo** ≫ **Eu** ≈ Si > Ca ≫ Fe > Al > Zn	19.0
	2.16	**Eu** > **Nd** ≫ **Mo** > Si ≫ Ca > Al > Fe > Zn	12.2
	2.79	**Nd** ≫>> **Eu** >>>**Mo** >> Si >>Zn > Fe > Ca > Al	54.1
	3.48	**Nd** ≫ **Eu** ≫>> **Mo** >> Zn > Si > Fe > Ca > Al	42.4
	3.86	**Eu** ≈ **Nd** ≫>> **Mo** > Fe >> Zn > Si > Ca > Al	56.0

Bold: target metals of the study.

Table 5
Sorbent recycling – Sorption and desorption performances for Nd(III) and Mo(VI) on P-APEI beads using 0.2 M HCl 0.5 M $CaCl_2$.

Cycle	Nd(III)				Mo(VI)			
	Sorption (%)		Desorption (%)		Sorption (%)		Desorption (%)	
	Average	S.D.	Average	S.D.	Average	S.D.	Average	S.D.
#1	97.7	0.4	100.1	0.1	98.1	0.2	100.5	0.0
#2	97.3	0.1	100.5	0.2	97.5	1.0	100.0	0.7
#3	96.7	0.5	100.9	0.1	96.1	0.5	100.6	0.0
#4	96.0	0.2	99.8	0.9	93.9	1.6	99.9	0.4
#5	95.6	0.3	100.4	0.7	93.0	2.3	100.4	0.2
Loss @ Run #5 (%)	2.2		negligible		5.3		negligible	

Table 6
Treatment of ore leachate.

Operation	Leaching		Cementation		Precipitation (pH 5)		Sorption efficiency (%)				
Parameter Metal	Conc. (mg L^{-1})	Leaching yield (%)	Conc. (mg L^{-1})	Removal (%)	Conc. (mg L^{-1})	Removal (%)	pH 1.28	pH 2.37	pH 3.21	pH 3.46	pH 3.89
Si(IV)	3479	2.13	3468	0.32	2157	37.80	0.86	1.26	1.54	1.67	2.32
Al(III)	24,075	44.35	24,000	0.31	179.35	99.25	0.69	1.88	5.77	6.71	7.70
Fe(III)	36,456	56.71	37,032	−1.58	64.90	99.82	1.37	18.69	30.82	33.79	38.18
Ca(II)	16,669	42.69	16,660	0.054	11,100	33.37	0.21	0.38	0.64	0.72	0.89
Mn(II)	3385.7	49.72	3369	0.49	2700	19.86	0.18	0.66	2.01	2.36	2.82
Ni(II)	107.24	86.62	98	8.62	81.06	17.29	0.20	2.39	10.32	20.95	25.49
Cu(II)	1428.3	95.22	11	99.23	6	45.45	n.s.	n.s.	n.s.	n.s.	n.s.
REE(III)	156.45	91.26	153	2.21	142	7.19	5.92	24.23	52.36	78.72	93.11
Nd (III)	49.78	n.d.	47.5	4.67	46.87	1.23	3.98	25.41	49.03	76.48	91.55
Eu(III)	28.77	n.d.	28	2.65	27.69	1.135	9.53	31.53	60.75	82.36	95.82
Mo(VI)	70.32	89.50	68	3.30	58	14.71	5.33	8.64	11.97	24.32	30.97
Zn(II)	53.31	95.68	48	9.96	39.90	16.88	2.23	2.48	6.81	12.02	17.85

n.s.: non-significant; n.d.: non-determined.

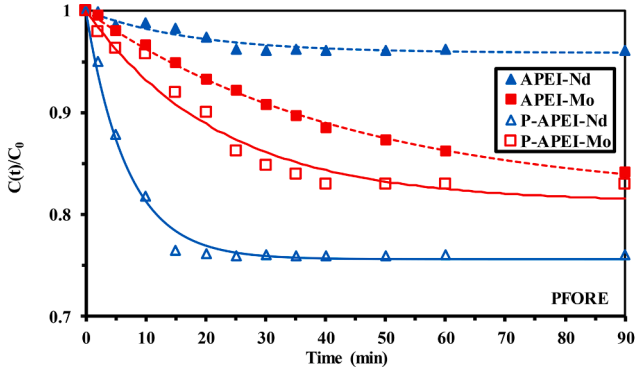

Fig. 4b. Uptake kinetics for Nd(III) and Mo(VI) from bi-component solutions using APEI and P-APEI beads (C_0: 50 or 500 mg mg L^{-1}; pH_0: 5, except for APEI/Mo(VI) system where pH_0 was set to 3; SD: 0.21 g L^{-1} for APEI and 0.3 g L^{-1} for P-APEI beads; T: 21 ± 1 °C; solid curves: modeling with the pseudo-first order rate equation).

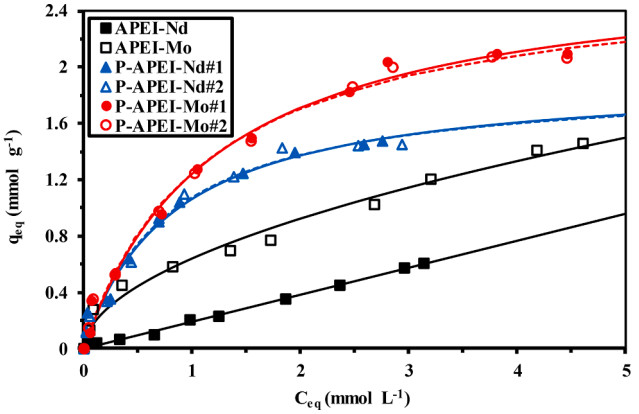

Fig. 5. Nd(III) and Mo(VI) sorption isotherms using APEI and P-APEI beads (C_0: 0.07–3.47 mmol Nd g^{-1}; 0.1–5.51 mmol Mo L^{-1}; pH_0: 5, except for APEI/Mo (VI) system where pH_0 was set to 3; SD: 0.4 g L^{-1}; T: 21 ± 1 °C; Contact time: 48 h; solid curves: Langmuir fit, except for APEI-Nd: linear relationship (Henry's Law) and APE-Mo: Freundlich equation).

properties.

3.2.3. *Sorption isotherms*

Fig. 5 shows Nd(III) and Mo(VI) sorption isotherms at pH_0: 5 (pH_0 3 for Mo(VI) and APEI sorbent). The superposition of the curves for P-APEI (Run #1 and #2) confirms the reproducibility of sorption performances for both Nd(III) and Mo(VI). Table 3 summarizes the parameters of the Langmuir, Freundlich and Sips equations for APEI and P-APEI sorbents. The experimental maximum sorption capacity for Nd(III) is significantly increased by phosphorylation: the sorption capacity increases by a factor close to 2.4. The TBP-derivative has a much lower impact on molybdate recovery: the sorption capacity is only increased by 43%. It is noteworthy that the isotherms of APEI sorbent are significantly different from those obtained with P-APEI. It is not possible finding an appropriate fit of experimental profiles using the three equations and the saturation plateau is not completed in the tested range of concentrations, especially for Nd(III). Actually, in the case of Nd(III), metal ions are linearly distributed between solid and liquid phase (the experimental points are linearly aligned, consistently with the Henry equation). For Mo(VI), the best fit was obtained with the Freundlich equation. For P-APEI sorbent, the trends are more marked: the Langmuir equation fits much better experimental profiles than the Freundlich and even the Sips equation (based on determination coefficients, AIC), regardless of the metal. However, the curves fail to fit the experimental points at low residual metal concentration (C_0 less than 0.2 mmol L^{-1}): sorption capacities are underestimated. The Langmuir equation

supposes that the sorption occurs: (a) as a monolayer at the surface of the sorbent, (b) without interactions between sorbed molecules, and (c) with a homogeneous distribution of sorption energy. The sorption capacities at saturation of the monolayer ($q_{m,L}$) exceed the maximum sorption capacities (by 40% for Nd(III) and 30% for Mo(VI)). The affinity coefficients (i.e., b_L) are a little higher for Nd(III) (1.25 ± 0.3 L mmol^{-1}) compared with Mo(VI) (i.e., 0.845 ± 0.3 L mmol^{-1}). The coefficient $q_{m,L} \times b_L$ (L g^{-1}, homogeneous to a distribution ratio) varies between 2.27 and 2.44 L g^{-1}. It is noteworthy that the type of metal hardly changes the value of this parameter. Actually, this coefficient corresponds to the initial slope of the isotherm curves; Fig. 3 confirms that this initial slope is roughly the same for Nd(III) and Mo(VI). It is noteworthy that the saturation plateau is only reached for concentrations as high as 3 mmol metal L^{-1}. P-APEI sorbent shows good sorption capacities for the two metal ions; although the affinity coefficient (b_L) remains relatively low. The sorption capacities at saturation of the monolayer are significantly lower than the molar content of reactive groups. Table 1 reports N and P contents of P-APEI (3.10 and 1.66 mmol g^{-1}, respectively); this means that phosphorus-bearing and free amine groups (not involved in the grafting of TBP derivative) represent 1.66 and 1.44 mmol g^{-1}, respectively. It is difficult connecting the maximum sorption capacities to the density of reactive groups and to determine a stoichiometric ratio between metal ions and individual (or combined) reactive groups. This may be explained by: (a) poor accessibility or availability of some of these functional groups, or (b) the simultaneous interaction of metal ions with distinct reactive groups (multidentate chelation or combination of binding process: ion-exchange and chelation).

Tables S4a and S4b summarizes the sorption properties of alternative sorbents for comparative evaluation of APEI and P-APEI sorbents for Nd (III) and Mo(VI), respectively. In the case of Nd(III), P-APEI sorbent shows one of the highest sorption capacities reported in the literature, only outperformed by magnetic glutamine PAN [51]. Faster kinetics partially compensate the relatively lower sorption capacity. Compared with other more conventional sorbents, P-APEI shows a combination of sorption properties (in terms of both uptake kinetics and sorption isotherms) that make the new material very attractive for neodymium recovery. In the case of Mo(VI), the sorption capacities are attractive and comparable to those of chitin- and chitosan-based sorbents [52,53], or DETA/PGME [54], Mo-imprinted composite [55]. Outstanding sorbents were reported using chitosan gel beads [56] or GMA/DVB/TEPA (sorption capacities in the range 6.6–8 mmol Mo g^{-1}) [57]; however, they usually require longer contact times for reaching equilibrium. The combination of the equilibrium and kinetics properties, associated with metal desorption and sorbent recycling performances (and selectivity) (see below) make this material very attractive as an alternative to these outstanding sorbents. Annex A (see Supplementary Information) compares the sorption properties (under comparable experimental conditions) of P-APEI beads with commercial resins Dowex 50X8 and Dowex HCR S/S (strong cation exchangers) (Figures A1-A3 and tables A1-A2). The new sorbent is characterized by much higher recovery of Nd(III) and Mo(VI) from both synthetic pure solutions and acidic leachates. Maximum sorption capacity for Nd(III) is more than 3 times higher, and about 10 times greater for Mo(VI) (Table A2). The lowest affinity of Dowex resins for Mo(VI) may explain the higher relative selectivity of the commercial resins for Nd(III) compared with P-APEI for the treatment of acidic leachates but at the expense of a drastic decrease in cumulative sorption capacities (3.85 mmol metal g^{-1} for P-APEI *vs.* 0.65–0.99 mmol metal g^{-1} for Dowex resins). These results confirm the promising perspectives opened by P-APEI for REEs recovery from complex solutions.

3.2.4. *Sorption mechanism*

Scheme 1 illustrated the suggested structure of the sorbent with identification of possible reactive groups; P-APEI is characterized as a multifunctional sorbent bearing phosphorus-based, hydroxyl, carboxylate, and amine groups. The data collected from FTIR, EDX, XPS analyses, and pH_{PZC} confirm that different mechanisms may be involved in the sorption of Nd(III) and Mo(VI), depending also on metal speciation. Hence, metal cations can be exchanged with Ca^{2+} and H^+ on alginate-based compounds in weakly acidic conditions, metal anions (molybdate more specifically) can be bound onto protonated amine groups in more acid solutions. Metal ions can be also chelated by amine or phosphate groups (including phosphomolybdate complexes). These different modes of binding have been characterized by shifts (and intensity changes) in the FTIR wavelengths and binding energies in HRES spectra. The speciation diagrams and the charges of the sorbent also bring support for explaining the affinity of the sorbent for target metals. Scheme 2 summarizes these different modes of interaction.

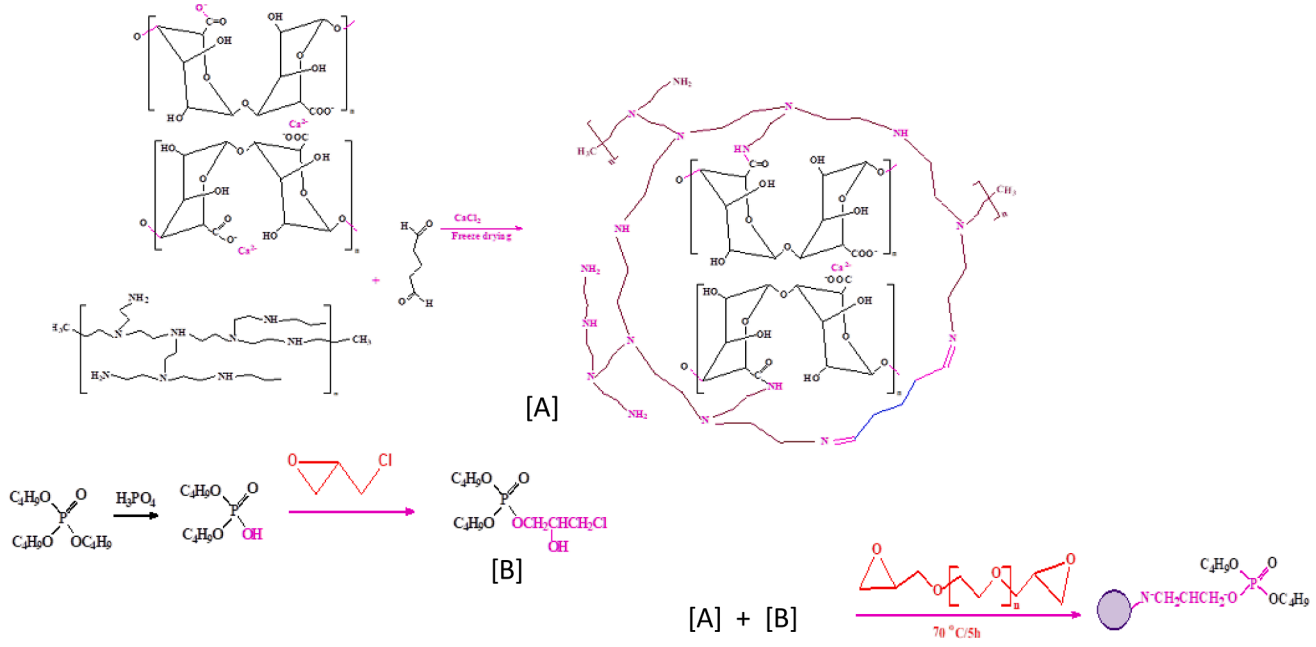

Scheme 1. Synthesis route for the functionalization of APEI (P-APEI).

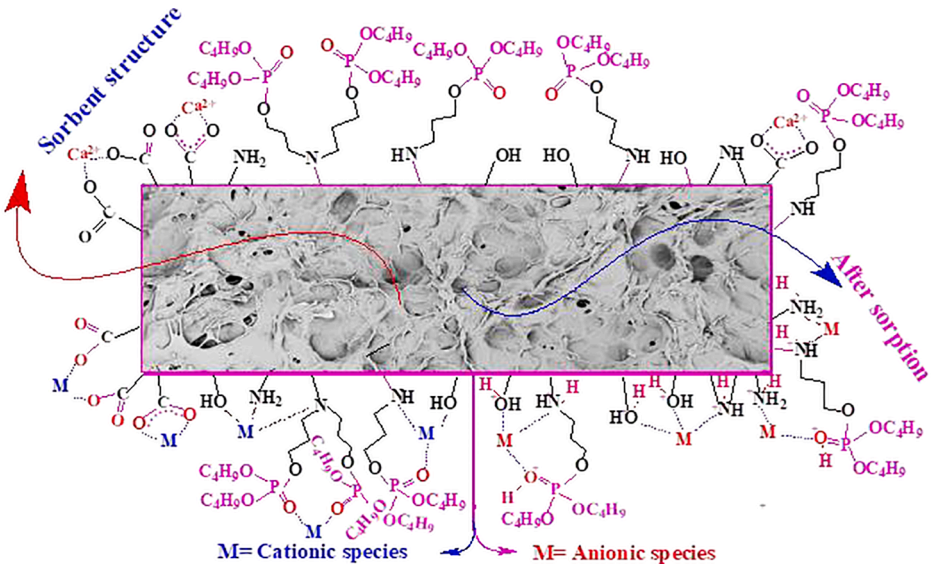

Scheme 2. Proposed modes of metal interactions with P-APEI sorbent.

3.2.5. Multi-component sorption – Selectivity

The sorption properties of APEI and P-APEI sorbents for Nd(III) and Mo(VI) were characterized at different pH values for multi-component equimolar solutions. Metal ions were selected for their frequent occurrence in the leaching of ores, including Al, Ca, and Si (for aluminosilicate basements), Fe and Zn (as conventional base metals, BMs), Mo (present in selected Egyptian ore), Nd and Eu (as representatives of Light and Heavy REEs). Fig. 6 shows the distribution ratio ($D = q_{eq}/C_{eq}$, L kg^{-1}), as a marker of the concentration effect of APEI and P-APEI at different equilibrium pH values. For the two sorbents, in most cases, the higher D

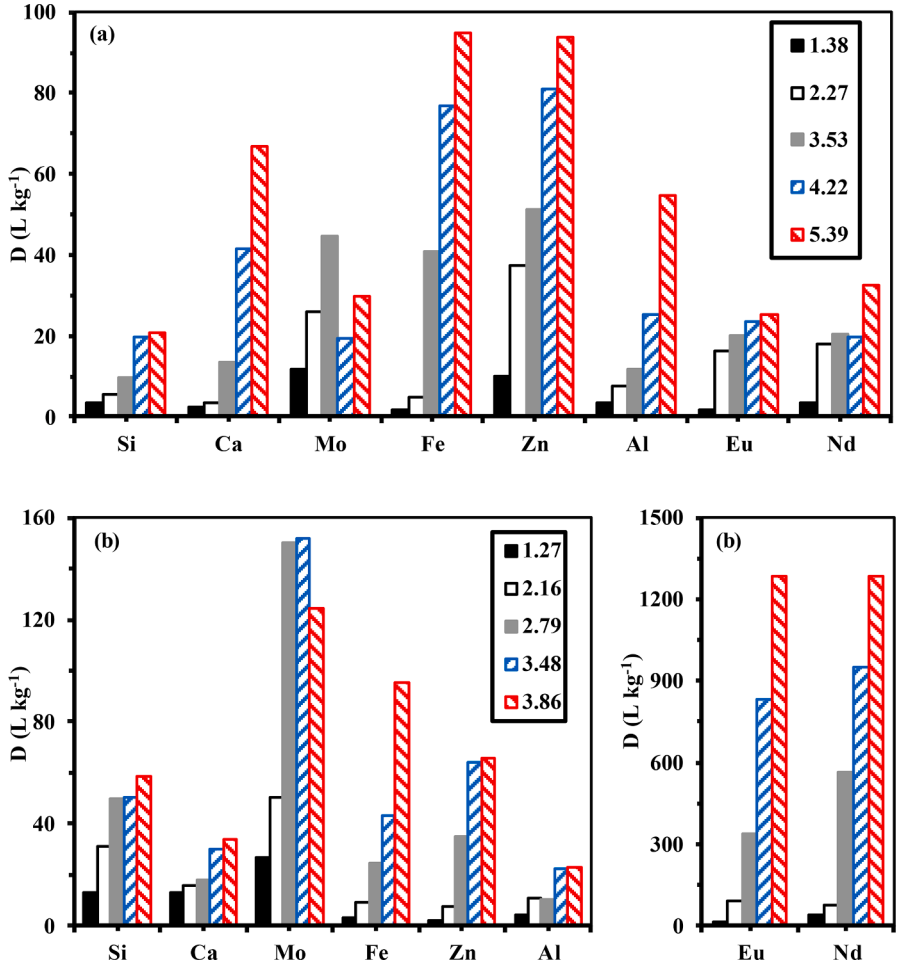

Fig. 611Effect of equilibrium pH on the distribution ratio for selected metal using APEI (a) and P-APEI (b) (C_0: 0.5 mmol metal L^{-1}; SD: 1.2 g L^{-1}; Contact time: 48 h).

values are obtained at the highest pH values. For APEI, the highest distribution ratios are observed for Fe, Zn, Ca and Al (up to 70–95 L kg^{-1}, under the most favorable conditions; i.e., at pH 5.39), contrary to Mo, Eu and Nd. The main reactive groups on APEI (such as amine and carboxylic/carboxylate groups) may broadly interact with metal cations through chelation, especially at pH higher than 4.5. With the phosphorylation of APEI, the distribution ratios are considerably increased for Mo up to 152 L kg^{-1}, and even more (up to 1289 L kg^{-1}) for Nd and Eu at pH_{eq} 3.86. The functionalization of APEI brings high concentration factors to REEs (and Mo to a lesser extent) *vs.* base metals; contrary to APEI that concentrates more significantly BMs (especially at pH_{eq} 4.22–5.39). APEI contains both hard O-donor groups (carboxylate moieties of alginate) and soft N-donor groups (primary, secondary and tertiary amine groups). The sorbent can bind both soft and hard acids (including borderline metal ions). The phosphorylation brings additional phosphate-like groups, which are hard bases. The grafting of TBP derivatives on amine groups of APEI decreases both the relative density of free (available and accessible) amine groups while O-donor groups of phosphate-based moieties increase the global number of O-donor groups: the sorption of REEs is favored by the phosphate-based groups. The softness parameters for Eu^{3+}, Nd^{3+}, Ca^{2+} and Al^{3+} are − 0.19, −0.66, −0.3 and −0.58, respectively [50], contrary to Fe^{3+} and Zn^{2+} that have positive values: +0.33 and + 0.35, respectively. Therefore, there is a rough correlation between the positive *vs.* negative values of softness parameter and their affinity for APEI or P-APEI, respectively. The softness parameter for phosphate ligand is close to −0.78 [50].

Table 4 ranks the distribution ratios of the different metal ions at the different pH values for APEI and P-APEI. The ratio D_{max}/D_{min} gives for each pH value the highest selectivity coefficient between the metals having the highest and the lowest affinities for the sorbent. The $SC_{M1/M2}$ coefficient is defined as the ratio of the distribution ratios D_{M1}/D_{M2}. This table confirms the conclusions reached in the discussion of Fig. 7. At pH 4.22–5.39, APEI preferentially binds BMs against REEs and Mo(VI). On the opposite hand, for P-APEI sorbent Mo(VI) and REEs are readily separated from BMs; however, the highest separations are reported for pH 2.79–3.86. Taking into account the order of magnitude of the distribution ratios at the different pH values the best chances for achieving the selective separation of the three metals from BMs would be obtained at pH 2.79 using P-APEI in column systems. Long columns would contribute to chromatographically enriching collected fractions with individual metals.

Fig. S9 shows the comparison of selectivity coefficients $SC_{Nd/metal}$ and $SC_{Mo/metal}$ for APEI and P-APEI at different equilibrium pH values. APEI preferentially separates Nd(III) from Si(IV), Ca(II), Fe(III) and Al (III) at pH 2.27 (with relatively low SC values: in the range 2.3–5.3). On the opposite hand, the sorbent does not show significant selectivity between Nd(III) and Eu(III), while the sorbent preferentially binds Zn(II) whatever the pH. Considering Mo(VI), the highest selectivities against other metals are obtained in strong acid solutions (i.e., pH 1.38–2.27) for APEI. The most easily separated metal ions are Ca(II), Fe(III), Si(IV), Al(III), Eu(III) and Nd(III) with highest values ranging between 3.3 and 7.6. However, the SC value is close to 1 against Zn(II): the two metal ions are equally bound to APEI. Surprisingly, molybdate is considered as a hard acid while Zn(II) is ranked among borderline metal ions. Other parameters are probably involved in the control of sorption performance such as the acid/base and speciation properties of respective metal ions.

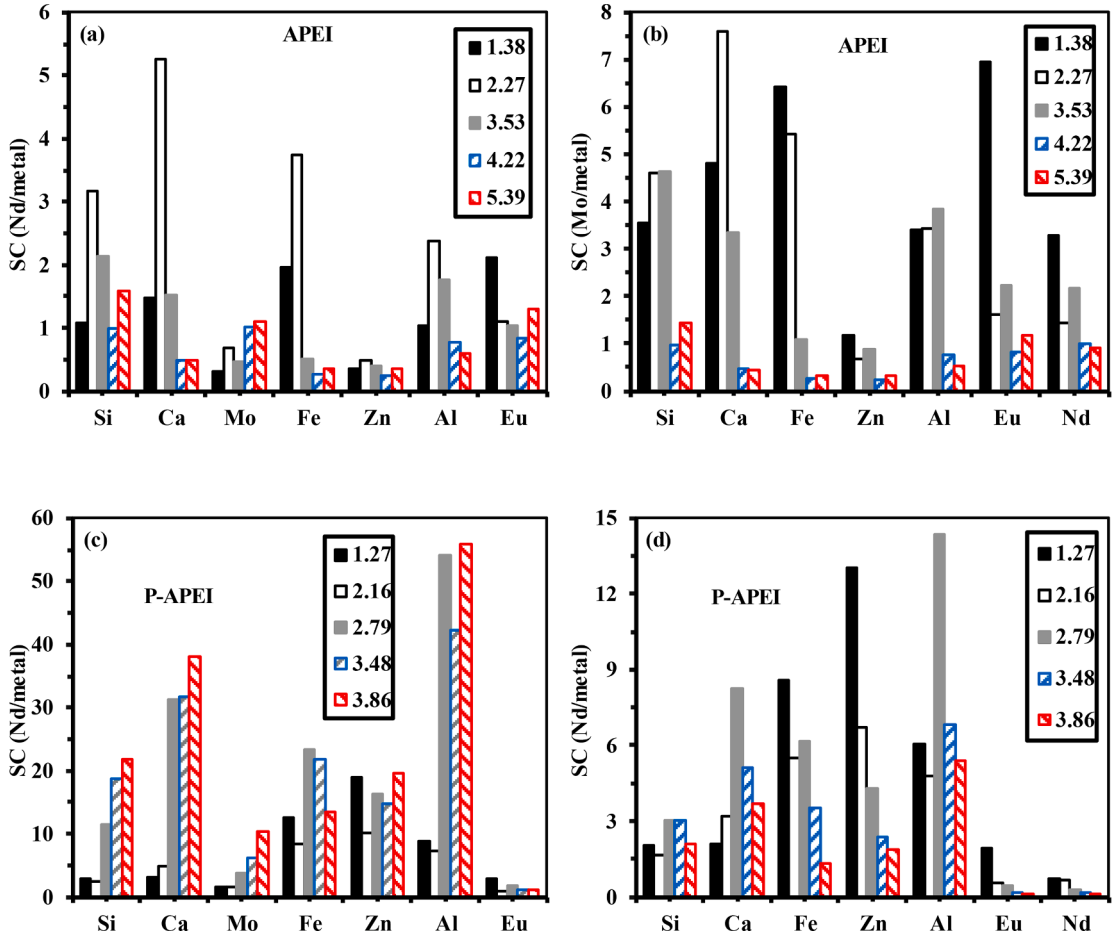

Fig. 7. Effect of pH on the selectivity coefficient for target metals (Nd(III): (a) and (c); and Mo(VI): (b) and (d)) using APEI and P-APEI beads (C_0: 0.5 mmol metal L^{-1}; SD: 1.2 g L^{-1}; Contact time: 48 h).

In the case of P-APEI sorbent, the order of magnitude of SC is increased, showing the highest separation power of the functionalized sorbent especially for Nd(III) selective binding. First, Nd(III) and Eu(III) cannot be separated; the two REEs are equally bound on P-APEI with limited effect of pH. The highest separation of the two metals is obtained at pH 2.79; however, the $SC_{Nd/Eu}$ does not exceed 1.67. A higher selectivity (i.e., 2.83) is obtained at pH 1.27 but at the expense of more competition from Si(IV) and Mo(VI). For most of the other metals (i.e., Al(III) > Ca (II) > Si(IV) > Zn(II) > Mo(VI)), the highest SC values are recorded at pH 3.86: SC varies between 10.3 and 56. In the case of Fe(III), the optimum separation is obtained at pH 2.79 ($SC_{Nd/Fe} \sim 21.9$). Nd(III) and Eu(III) can be selectively recovered from weakly acidic solutions using P-APEI. Regarding the separation of Mo(VI) from Al(III), Ca(II) and Si(IV), the best pH is found at pH 2.79 (14 > SC greater than 3), while the separation from Zn(II) and Fe(III) is optimum at pH 1.27 (SC: 13.1–8.6). It is noteworthy that Mo(VI) cannot be separated from Eu(III) and Nd(III): the highest SC (close to 1.95 and 0.8, respectively) are obtained at pH 1.27; at higher pH, the sorbent has a marked preference for REEs *vs.* Mo (VI).

Fig. S10 compares the molar fractions of the different metals at different pH values for APEI and P-APEI. While APEI binds high relative fractions of different metals and poor separation, P-APEI shows a marked preference for our target metal ions: Nd(III), Eu(III) and Mo(VI). In the range of pH 2.79–3.86, the three metals represent about 83–80% of total sorption. At pH 3.86, Eu(III) and Nd(III) are almost equally accumulated on the sorbent and the cumulative fraction of REEs on the sorbent is close to 72%. These two pH values offer either optimal sorption of target metals (i.e., pH 2.79) or optimal separation of REEs (i.e., pH 3.86).

Fig. S11 shows the effect of the pH on the cumulative sorption capacity using APEI and P-APEI (multi-component solutions). The cumulative sorption capacities are significantly lower than the values collected from sorption isotherms: $C_{eq,cumul}$: ≈ 7 mmol metal L^{-1} and q_{eq}: 1.25–1.44 mmol g^{-1} *vs.* 1.45 mmol Nd g^{-1} and 2.07 mmol Mo g^{-1} for mono-component solutions and residual metal concentrations in the range 4–5 mmol metal L^{-1}. The complementary sorption of BMs at pH 4.22–5.39 using APEI increases sorption capacity that remains much lower than the values reached for mono-component solutions (see sorption isotherms).

For a global valorization of multi-metals from complex solution, the selectivity could be completed by optimized desorption and further selective oxalate precipitation of REEs.

3.2.6. *Metal desorption and sorbent recycling*

Fig. S12 compares the kinetic profiles for the desorption of Nd(III) and Mo(VI) from P-APEI using different eluents: inorganic acids (HCl and HNO_3), citric acid (Fig. S12a), calcium chloride, sodium bicarbonate and sodium hydrogen carbonate (Fig. S12b). Two objectives are considered: optimizing metal desorption and eventually selecting an eluent that could be used for separating the two metals. Neodymium can be efficiently desorbed by inorganic acid: the complete elution of the REE is achieved within 60 min for both HCl and HNO_3 and the profiles are perfectly superposed. On the opposite hand, metal desorption does not exceed 94% after 600 min of contact with citric acid, 65% with $CaCl_2$. Sodium carbonate completely desorb Nd(III) within 120 min of contact while the desorption yield does not exceed 95% with sodium hydrogen carbonate. It is noteworthy that high concentrations of sodium may cause the partial degradation of the sorbent dues to calcium ion exchange of alginate moieties to form soluble sodium alginate. On the opposite hand, calcium-based solutions may improve the stability of the material at the expense of a decrease in desorption performance. In the case of Mo(VI), metal desorption does not exceed 73% and 82% (after 120 min of contact) with HCl and HNO_3, respectively. Desorption yield is even worst in the case of citric acid (i.e., about 42% after 600 min). The best desorption is achieved with sodium carbonate (i.e., about 95%, in 120 min); better than with $NaHCO_3$ (i.e., 84% in 600 min) or $CaCl_2$ (i.e., almost 34% after 600 min). These data show that mineral acid are the most appropriate for eluting Nd(III) while Na_2CO_3 is more appropriate for Mo(VI) desorption. The separation effects associated with these different eluents are not expected to be high enough for justifying the use of different eluents for Nd(III) and Mo(VI). The sensitivity of the sorbent to the presence of high concentrations of sodium suggests using HCl solutions for the desorption of the two metals; in order to reinforce its stability for recycling, the 0.2 M HCl solution may be completed by addition of $CaCl_2$ (0.5 M), since calcium ions contribute to the regeneration of the linkages by ionotropic gelation. The impact of the eluents on the structure (morphology, porosity) of P-APEI beads has been characterized using SEM (Fig. S13a-c). Apparently, the use of the eluents influences the surface morphology by creating heterogeneities (small folds for 0.2 M HCl, 0.5 M $CaCl_2$, 0.5 M Na_2CO_3), pores (0.2 M HNO_3, 0.5 M $NaHCO_3$); citric acid (0.5 M) has a limited effect on surface topography. The internal scaffold is hardly changed, except for 0.5 M Na_2CO_3, where the folds seem to be swelled and the internal surface covered by irregular deposits. These observations tend to confirm that the use of HCl and $CaCl_2$ has a negligible impact on the morphology of beads.

Fig. S14a and b compares the kinetics of desorption for APEI and P-APEI for beads collected during uptake kinetics at different concentrations (see Section 3.2.2), using 0.2 M HCl/0.5 M $CaCl_2$ eluent. For Nd (III), the profiles of desorption are very close for APEI and P-APEI, and hardly affected by metal loading: the desorption of both Nd(III) and Mo (VI) is completed and achieved within 15–25 min of contact. In the case of Mo(VI), 25–30 min are necessary for achieving the complete elution of the two metals. Apparently, the desorption is little faster for APEI compared with P-APEI (especially at low metal loading). This eluent is highly efficient both in terms of elution yield and kinetics for the recovery of REE(III) and Mo(VI) from loaded sorbents.

Table 5 reports the sorption and desorption yields for five successive cycles of sorption and desorption for P-APEI sorbent. The performances are remarkably stable: the loss in sorption does not exceed 2.2% for Nd (III) and 5.3% for Mo(VI) at the fifth cycle. On the opposite hand, the desorption efficiency is not influenced by recycling steps: the yield systematically exceed 99%. This stability is consistent with the restoration of FTIR spectra after metal elution, as reported above (Fig. 1, Section 3.1.2).

The SEM observation of the two sorbents at different stages of their uses (i.e., after the sorption and the desorption of the metal ions) is shown in Fig. S13a-c. The pictures clearly show that the processing of APEI beads affects the surface morphology of the beads with creation of relatively large pores (10–30 μm, larger for beads in contact with Mo (VI)). Cross-cut sections do not show substantial changes, except for Nd (III) where scaffold breaks can be identified. For P-APEI, the surface and internal structures are not affected by the sorption and the desorption of the metal ions: the most significant changes are detected for Nd(III) sorption steps, where again some broken scaffolds are observed. Table S5 compares the semi-quantitative analyses of beads (raw, after the sorption of metals and after metal desorption). Metal binding is accompanied by the appearance of Nd and Mo elements: as expected Mo (VI) sorption is higher than Nd(III) and P-APEI is more efficient than APEI. For APEI beads, the atomic percentages are comparable at the surface and in the core of the sorbent for Nd(III) uptake, while Mo(VI) accumulates more efficiently in the core of the beads. In the case of P-APEI beads, the surface concentration for both Nd(III) and Mo(VI) is higher at the surface of the beads than in the internal compartment. The desorption is highly efficient because the metals are not detected in the eluted materials. Neodymium sorption is followed by the relative decrease of Cl content (ion-exchange) and the increase of S content (probably associated with sulfate binding from the acid and/or neodymium as sulfate species). After metal desorption, the contents of Cl and Ca increase due to ion-exchange on protonated amine groups and carboxylate groups, respectively. Surprisingly, the P content increases with metal sorption and desorption, while N content decreases in the

case of Mo(VI) processing.

3.3. Ore processing and metal recovery

3.3.1. Ore leaching and pre-treatment of leachates

The pug leaching of the ore generated a multi-metal solution containing high concentration of iron, aluminum and copper that can affect the sorption properties and saturate the sorbent. In addition, the separation of these metals from target metals prior to sorption step on P-APEI may contribute to enhance the selective recovery of Mo(VI) and Nd(III). For these reasons, a series of pre-treatments was used including Cu cementation (using iron) and a precipitation step at pH 5. The detailed effects of these treatments on the composition of the leachates is fully documented in the Supplementary Information section (in Annex B). As expected the cementation process strongly reduce copper concentration: more than 99% of copper is recovered as cementate (at the expense of an increase in iron concentration in the leachate). The precipitation step allows removing more than 99% of both iron and aluminum. Table 6 reports the detailed concentrations of selected metals at the different steps in the pre-treatment process and the solution effectively submitted to the sorption step on P-APEI.

3.3.2. Sorption processing

Table 6 also reports the sorption efficiency for selected metals at different equilibrium pH values while using P-APEI sorbent. Regardless of the metal, the sorption efficiency increases with pH. However, the sorbent shows a marked preference for REEs. At pH 3.89, considering individually Nd(III) and Eu(III) or globally (as the composite global index), the sorption efficiency exceeds 91.5%, while for other base metals the recovery varies between 38.2% (for iron) and 17.8% (for zinc); the recoveries of nickel and molybdenum stand to 25.5% and 31%, respectively. On the other side, the removal efficiency for other base metals ranges between 0.9% (calcium) and 7.7% (aluminum). These results confirm previous conclusions from selectivity tests: P-APEI sorbent has a marked preference for REEs while Mo(VI) is much less sorbed (at a level comparable to other heavy metal ions).

Fig. S15 compares the distribution ratios of selected metals at pH_{eq} 2.7 and 3.89. This figure clearly illustrates the importance of pH (pH_{eq} 3.89) and the high affinity of the sorbent for Nd(III) and Eu(III) compared with other metals present in the complex solution (D close to 23 for Eu(III), and to 11 for Nd(III)). This is confirmed by the enrichment factor (EF defined as the molar fraction of the metal in the sorbent against its molar fraction in the initial solution). The EFs values are close to 0.92–0.96 for the REEs while the values are much lower for Zn(II) (0.178) < Ni(II) (0.255) < Mo(VI) (0.310); for other metals, the EF is systematically below 0.08. This is also confirmed by the selectivity coefficient $SC_{Nd/metal}$. Close to 1, the $SC_{Nd/Eu}$ parameter demonstrates that the two metals cannot be readily separated by the sorbent. Under selected experimental conditions, the selectivity increases according the series: Fe(III) < Mo(VI) < Ni(II) < Zn(II) < Al(III) < Mn(II) < Si(IV) < Ca (II) through the combined influence of selectivity and metal concentration effect.

Table S6 reports the semi-quantitative surface analysis of P-APEI beads after sorption step at pH 3.89. All the members of the complete family of REEs (including chemical analogues such as Y and Sc) are significantly bound on the sorbent with atomic percentages varying between 0.33% and 1.32% (weight percentage 1.0–5.6%). The total weight fraction of the REEs is close to 41%. Fig. 8 and Fig. S16 show the distribution of the metals in the different compartments (cementate, precipitate, sorbent and residual solution). Copper(II) is almost completely recovered in the cementate. The semi-quantitative EDX analysis of the cementate shows that impurities represent less than 3% (weight). Al(III) and Fe(III) are mainly recovered in the precipitate, as expected from the rationale of these successive operative steps.

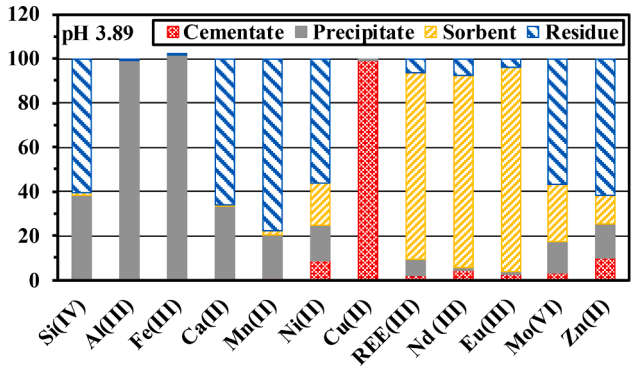

Fig. 8. Distribution of selected metals in the different compartments (cementate, precipitate, sorbent (P-APEI) and residual solution) at different pH values (pH 3.89, complement to Fig. S16).

3.3.3. Elution and valorization

The elution of the sorbent was performed using 0.2 M HCl/0.5 M $CaCl_2$ solution and the eluate was treated by oxalic acid precipitation at pH 1.1 [58–61]. The semi-quantitative analysis of desorbed sorbent shows that the desorption yield exceeds 98% for REEs. The precipitate collected after REEs oxalate precipitation were semi-quantitatively analyzed by SEM-EDX (Table S7). While the atomic percentages of REEs on the sorbent varied in the range 0.33–1.32% (Table S7), the oxalate precipitate shows much larger differences in the distributions of the REEs (from 0.11% for Ho(III) and up to 6.43% for Nd(III)). Some traces of Ca(II) are also detected (i.e., 0.6%). The total atomic fraction in the precipitate reaches up to 13% (i.e., 51% in weight). A final step of calcination would produce a concentrate of REEs oxides [62]. Globally, the process allows separating REEs from BMs. The residual traces of calcium could be removed by weak acidic leachate.

The significant differences in the atomic distribution of the REEs between sorbent and oxalate precipitate are discussed by the comparison of the relative ratio of individual REEs (compared with total REEs) in the two compartments against atomic weight, hydrated radius (HR) and solution-phase electronegativity (χ) (Fig. S17). Apparently, the enrichment of REEs is enhanced when the hydrated radius is set between 1.05 and 1.19 Å and the χ coefficient varies between 3 and 3.4. Since EDX only provides a semi-quantitative evaluation of relative concentrations, these trends should be considered as indicative but they open interesting perspectives for the development of processes for selective separation of REEs.

The Scheme B1 (Annex B) proposes a tentative flow sheet for the global treatment of the ore.

4. Conclusions

Algal-PEI beads (APEI) have intrinsic sorption properties for metal sorption due to the presence of carboxylic and amine groups. The functionalization of their surface by grafting new reactive groups allows improving the sorption performances as already demonstrated with quaternization or the insertion of sulfonic groups. The immobilization of a TBP derivative allows phosphorylating APEI beads and substantially increasing Nd(III) maximum sorption capacity (from 0.61 to 1.46 mmol Nd g^{-1}): strong interactions between phosphate and Nd(III) are identified. The enhancement of Mo(VI) uptake is much less marked (from 1.46 to 2.09 mmol Mo g^{-1}) because of the naturally high affinity of molybdate species for amine groups. These trends are confirmed by the identification of interaction modes using FTIR and XPS analyses. The effect of pH (optimum at pH 3–4) also contributes to explain these mechanisms through its impact on metal speciation and in relation with the overall charge of sorbent surface (pH_{PZC}).

Despite its low specific surface area, P-APEI sorbent shows fast sorption: the equilibrium time is reached within 30–40 min of contact.

The kinetic profiles are well fitted by the pseudo-first order rate equation. The phosphorylation does not change the mass transfer properties and the apparent rate coefficients for both Nd(III) and Mo(VI) (parameters are of the same order of magnitude). It is noteworthy that the effective diffusivity is close to the self-diffusivity of these metals as a confirmation of the limited effect of resistance to intraparticle diffusion on overall uptake kinetics. The sorption isotherms are well fitted by the Langmuir equation. The comparison of maximum sorption capacity of P-APEI for Nd(III) allows classifying this sorbent among the most efficient reported in literature. The comparison of sorption performances with two commercial resins (Dowex 50X8 and Dowex HCR S/S) confirm the superiority of this new sorbent.

Different eluents have been tested for the recovery of Nd(III) and Mo (VI) from loaded sorbents. In terms of desorption kinetics, recovery efficiency and sorbent stability (SEM observations), the best eluent is constituted of a mixture of HCl (0.2 M) and $CaCl_2$ (0.5 M). Thirty minutes of contact are sufficient for completely eluting the two metal ions. This high desorption efficiency is maintained for at least 5 cycles, while the sorption efficiency decreases by only 2–5% at the fifth cycle.

The functionalized sorbent has a marked preference for rare earths in multi-component synthetic solutions against alkali-earth and base metals, especially at pH higher than 2.7. This affinity for rare earths is confirmed in the treatment of acidic leachates of Egyptian ores. Sulfuric acid leaching produces multi-metal solutions that are successfully pre-treated by cementation (for selective Cu recovery), precipitation (for Fe and Al abatement). After control of the pre-treated solution at pH close to 3.8, P-APEI efficiently binds and concentrates the rare earth elements that can be recovered by elution before being selectively precipitated with oxalic acid. The enrichment factor calculated after oxalate precipitation shows a marked preference for Nd > Sm > Gd > Eu > Pr > Dy (correlated with favorable hydrated radius and solution phase electronegativity windows). The sorbent shows much higher selectivity for Mo(VI) recovery from complex pre-treated leachate, while the selectivity is less marked for Nd(III). However, the sorption capacities are significantly higher for P-APEI compared with Dowex resins (3.85 mmol metal g^{-1} *vs.* 0.65–0.99 mmol g^{-1})

Apparently, P-APEI shows high and attractive sorption performances for the recovery of rare earth elements. Next step will consist in testing the sorption performances in fixed-bed columns with evaluation of the possibility to enhance the chromatographic separation of rare earth elements.

Declaration of Competing Interest

The authors declare that they have no known competing financial interests or personal relationships that could have appeared to influence the work reported in this paper.

Acknowledgements

Y. W. thanks the support of NSFC (National Natural Science Foundation of China) Projects (No. 11675102, No. 11975082, U1967218), Science and Technology Major Project of Guangxi Province (China) (AA17204100, AA18118030). E.G. acknowledges the support from Institut Français d'Egypte (France) for sustaining the collaboration between IMT Mines Ales and Egyptian Institutions and Universities (including NMA). E.G. and M.F.H. thank the financial support of the IMHOTEP project "MetalValor" (ref. 39529QA) (Ministère des Affaires Etrangères, Ministère de l'Enseignement Supérieur et de la Recherche (France) and the Science and Technology Development Fund (Egypt)).

Appendix A. Supplementary data

Supplementary data to this article can be found online at https://doi.org/10.1016/j.cej.2020.127399.

References

[1] S. Pavon, A. Fortuny, M.T. Coll, A.M. Sastre, Neodymium recovery from NdFeB magnet wastes using Primene 81R.Cyanex 572 IL by solvent extraction, J. Environ. Manage. 222 (2018) 359–367.
[2] R.Z. Rebello, M.T.W. Dias Carneiro Lima, L.H. Yamane, R.R. Siman, Characterization of end-of-life LED lamps for the recovery of precious metals and rare earth elements, Resour. Conserv. Recycl. 153 (2020).
[3] S. Pavon, A. Fortuny, M.T. Coll, A.M. Sastre, Rare earths separation from fluorescent lamp wastes using ionic liquids as extractant agents, Waste Manage. (Oxford) 82 (2018) 241–248.
[4] D.D. Miller, R. Siriwardane, D. McIntyre, Anion structural effects on interaction of rare earth element ions with Dowex 50W X8 cation exchange resin, J. Rare Earths 36 (2018) 879–890.
[5] D. Kolodynska, D. Fila, Z. Hubicki, Evaluation of possible use of the macroporous ion exchanger in the adsorption process of rare earth elements and heavy metal ions from spent batteries solutions, Chem. Eng. Process. Process Intensif. 147 (2020).
[6] D. Kolodynska, D. Fila, Z. Hubicki, Recovery of lanthanum(III) and nickel(II) ions from acidic solutions by the highly effective ion exchanger, Molecules, 25 (2020) Art. N° 3718.
[7] D. Fila, Z. Hubicki, D. Kolodynska, Recovery of metals from waste nickel-metal hydride batteries using multifunctional Diphonix resin, Adsorption (J. Int. Ads. Soc.) 25 (2019) 367–382.
[8] J.C. Callura, K.M. Perkins, J.P. Baltrus, N.R. Washburn, D.A. Dzombak, A. K. Karamalidis, Adsorption kinetics, thermodynamics, and isotherm studies for functionalized lanthanide-chelating resins, J. Colloid Interface Sci. 557 (2019) 465–477.
[9] S. Mondal, A. Ghar, A.K. Satpati, P. Sinharoy, D.K. Singh, J.N. Sharma, T. Sreenivas, V. Kain, Recovery of rare earth elements from coal fly ash using TEHDGA impregnated resin, Hydrometallurgy 185 (2019) 93–101.
[10] T. Kegl, A. Kosak, A. Lobnik, Z. Novak, A.K. Kralj, I. Ban, Adsorption of rare earth metals from wastewater by nanomaterials: a review, J. Hazard. Mater. 386 (2020).
[11] F.J. Alguacil, I. Garcia-Diaz, E. Escudero Baquero, O. Rodriguez Largo, F.A. Lopez, Oxidized and non-oxidized multiwalled carbon nanotubes as materials for adsorption of lanthanum(III) aqueous solutions, Metals 10 (2020).
[12] B. Maranescu, L. Lupa, A. Visa, Synthesis, characterization and rare earth elements adsorption properties of phosphonate metal organic frameworks, Appl. Surf. Sci 481 (2019) 83–91.
[13] M. Butnariu, P. Negrea, L. Lupa, M. Ciopec, A. Negrea, M. Pentea, I. Sarac, I. Samfira, Remediation of rare earth element pollutants by sorption process using organic natural sorbents, Int. J. Environ. Res. Public Health 12 (2015) 11278–11287.
[14] L. Alcaraz, M.E. Escudero, F.J. Alguacil, I. Llorente, A. Urbieta, P. Fernandez, F. A. Lopez, Dysprosium removal from water using active carbons obtained from spent coffee ground, Nanomaterials 9 (2019).
[15] B. Lapo, J.J. Bou, J. Hoyo, M. Carrillo, K. Pena, T. Tzanov, A.M. Sastre, A potential lignocellulosic biomass based on banana waste for critical rare earths recovery from aqueous solutions, Environ. Pollut 264 (2020).
[16] H. Javadian, M. Ruiz, M. Taghavi, A.M. Sastre, Synthesis of magnetic CMC bionanocomposite containing a novel biodegradable nanoporous polyamide selectively synthesized in ionic liquid as green media: Investigation on Nd+3, Tb+3, and Dy+3 rare earth elements adsorption, J. Mol. Liq., 308 (2020) Art. N° 113017.
[17] S. Valverde Duran, B. Lapo, M. Meneses, A. Maria Sastre, Recovery of neodymium (III) from aqueous phase by chitosan-manganese-ferrite magnetic beads, Nanomaterials 10 (2020).
[18] Y. Wei, K.A.M. Salih, S. Lu, M.F. Hamza, T. Fujita, T. Vincent, E. Guibal, Amidoxime functionalization of algal/polyethyleneimine beads for the sorption of Sr(II) from aqueous solutions, Molecules, 24 (2019) Art. N° 3893.
[19] M.F. Hamza, S.M. Lu, K.A.M. Salih, H. Mira, A.S. Dhmees, T. Fujita, Y.Z. Wei, T. Vincent, E. Guibal, As(V) sorption from aqueous solutions using quaternized algal/polyethyleneimine composite beads, Sci. Total Environ., 719 (2020) Art. N° 137396.
[20] M.F. Hamza, A.E. Mubark, Y. Wei, T. Vincent, E. Guibal, Quaternization of composite algal/PEI beads for enhanced uranium sorption-application to ore acidic leachate, Gels, 6 (2020) Art. N° 6020012.
[21] M.F. Hamza, K.A.M. Salih, A.A.H. Abdel-Rahman, Y.E. Zayed, Y. Wei, J. Liang, E. Guibal, Sulfonic-functionalized algal/PEI beads for scandium, cerium and holmium sorption from aqueous solutions (synthetic and industrial samples), Chem. Eng. J., 403 (2021) Art. N° 126399.
[22] A. Senol, Liquid-liquid extraction of uranium(VI) from aqueous acidic solutions using Alamine, TBP and CYANEX systems, J. Radioanal. Nucl. Chem. 258 (2003) 361–372.
[23] M. Ghadiri, S.N. Ashrafizadeh, M. Taghizadeh, Study of molybdenum extraction by trioctylamine and tributylphosphate and stripping by ammonium solutions, Hydrometallurgy 144 (2014) 151–155.
[24] Y. Li, Z. Zhao, Separation of molybdenum from acidic high-phosphorus tungsten solution by solvent extraction, Jom 69 (2017) 1920–1924.
[25] P. Tkac, M.A. Momen, A.T. Breshears, M.A. Brown, G.F. Vandegrift, Molybdenum (VI) coordination in tributyl phosphate chloride based system, Ind. Eng. Chem. Res. 57 (2018) 5661–5669.
[26] S.S. Chikkamath, D.M. Patil, A.S. Kabadagi, V.S. Tripathi, A.S. Kar, J. Manjanna, Recovery of molybdenum by solvent extraction from simulated high level liquid waste, J. Radioanal. Nucl. Chem. 321 (2019) 1027–1034.

[27] K. Sawada, D. Hirabayashi, Y. Enokida, Fundamental studies on extraction of actinides from spent fuels using liquefied gases - Conversion of copper into nitrate with NO2 and extraction of Nd(III) nitrate by CO2 with TBP, Prog. Nucl. Energy 50 (2008) 483–486.
[28] T. Vincent, M. Mukhopadhay, P.K. Wattal, Supercritical direct extraction of neodymium using TTA and TBP, Desalination 232 (2008) 91–101.
[29] A.T. Naeem, E. Kashi, M.A. Salehi, R. Habibpour, Extraction and separation of La (III), Pr(III) and Nd(III) using binary mixture of D2EHPA with Cyanex272, TOPO, and TBP extractants, Metall. Res. Technol. 115 (2018).
[30] H. Wang, X.-Z. Shao, Q. Tian, Y.-Q. Ji, Synthesis of TBP-coated magnetic Pst-DVB particles for uranium separation, Nucl. Sci. Tech. 25 (2014).
[31] K.V. Mares, F. Sebesta, Properties of PAN-TBP extraction chromatographic material, J. Radioanal. Nucl. Chem. 302 (2014) 341–345.
[32] J. Florek, S. Giret, E. Juere, D. Lariviere, F. Kleitz, Functionalization of mesoporous materials for lanthanide and actinide extraction, Dalton Trans. 45 (2016) 14832–14854.
[33] X. Guo, Y. Feng, L. Ma, D. Gao, J. Jing, J. Yu, H. Sun, H. Gong, Y. Zhang, Phosphoryl functionalized mesoporous silica for uranium adsorption, Appl. Surf. Sci 402 (2017) 53–60.
[34] S. Wang, T. Vincent, C. Faur, E. Rodriguez-Castellon, E. Guibal, A new method for incorporating polyethyleneimine (PEI) in algal beads: high stability as sorbent for palladium recovery and supported catalyst for nitrophenol hydrogenation, Mater. Chem. Phys. 221 (2019) 144–155.
[35] Z. Marczenko, M. Balcerzak, Chapter 39 – Rare-earth elements, in: Z. Marczenko, M. Balcerzak (Eds.), Analytical Spectroscopy Library, Elsevier, 2000, pp. 341–349.
[36] Z. Alothman, A review: Fundamental aspects of silicate mesoporous materials, Materials 5 (2012) 2874–2902.
[37] R. Valentin, R. Horga, B. Bonelli, E. Garrone, F. Di Renzo, F. Quignard, FTIR spectroscopy of NH_3 on acidic and ionotropic alginate aerogels, Biomacromolecules 7 (2006) 877–882.
[38] R. Rodriguez-Dorado, C. Lopez-Iglesias, C.A. Garcia-Gonzalez, G. Auriemma, R.P. Aquino, P. Del Gaudio, Design of aerogels, cryogels and xerogels of alginate: Effect of molecular weight, gelation conditions and drying method on particles' micromeritics, Molecules, 24 (2019) Art. N° 24061049.
[39] R. Nazir, S. Gaan, Recent developments in P(O/S)-N containing flame retardants, J. Appl. Polym. Sci., 137 (2020) Art. N° 47910 (47927 p).
[40] C. Zhu, Y. Xia, Y. Zai, Y. Dai, X. Liu, J. Bian, Y. Liu, J. Liu, G. Li, Adsorption and desorption behaviors of HPEI and thermoresponsive HPEI based gels on anionic and cationic dyes, Chem. Eng. J. 369 (2019) 863–873.
[41] B.K. Sen, S. Tiwari, M.K. Deb, S. Pervez, Nanogram level quantification of molybdenum(vi) by novel hyphenated SDME/DRS-FTIR in human biological fluid, Anal. Methods 7 (2015) 9474–9481.
[42] S. Sadighi, S.K. Masoudian, Preparation of biofuel from palm oil catalyzed by ammonium molybdate in homogeneous phase, Bull. Chem. Recation Eng. Catal. 12 (2017) 49–54.
[43] S.E. Karekar, B.A. Bhanvase, S.H. Sonawane, M.P. Deosarkar, D.V. Pinjari, A. B. Pandit, Synthesis of zinc molybdate and zinc phosphomolybdate nanopigments by an ultrasound assisted route: Advantage over conventional method, Chem. Eng. Process. Process Intensif. 87 (2015) 51–59.
[44] A.V. Murugan, C.W. Kwon, G. Campet, B.B. Kale, Synthesis and characterization of novel organo-inorganic hybrid material of poly(3,4-ethylene dioxythiophene) and phosphomolybdate anion, Act. Passive Electron. Compon., 26 (2003) Art. N° 456152.
[45] K. Shakeela, S. Guru, G.R. Rao, Cationic dye adsorption by phosphomolybdate nanoclusters immobilised on polyelectrolyte matrix, J. Chem. Sci. 132 (2020).
[46] M.V. Lopez-Ramon, F. Stoeckli, C. Moreno-Castilla, F. Carrasco-Marin, On the characterization of acidic and basic surface sites on carbons by various techniques, Carbon 37 (1999) 1215–1221.
[47] Z. Zeng, S. Yang, L. Zhang, D. Hua, Phosphonate-functionalized polystyrene microspheres with controlled zeta potential for efficient uranium sorption, RSC Adv. 6 (2016) 74110–74116.
[48] E. Guibal, C. Milot, J. Roussy, Influence of hydrolysis mechanisms on molybdate sorption isotherms using chitosan, Sep. Sci. Technol. 35 (2000) 1021–1038.
[49] H. Katano, T. Ueda, Spectrophotometric determination of phosphate anion based on the formation of molybdophosphate in ethylene glycol-water mixed solution, Anal. Sci. 27 (2011) 1043–1047.
[50] Y. Marcus, Ion Properties, Marcel Dekker Inc, New York, NY, 1997, p. 259.
[51] M.F. Hamza, A.A.H. Abdel-Rahman, E. Guibal, Magnetic glutamine-grafted polymer for the sorption of U(VI), Nd(III) and Dy(III), J. Chem. Technol. Biotechnol. 93 (2018) 1790–1806.
[52] Y. Xiong, Y. Li, F. Ren, L. Wan, Z. Xing, Z. Lou, W. Shan, Optimization of Mo(VI) selective separation by *Eriocheir sinesis* crab shells gel, Ind. Eng. Chem. Res. 53 (2014) 847–854.
[53] F.A. Bertoni, J.C. Gonzalez, S.I. Garcia, L.F. Sala, S.E. Bellu, Application of chitosan in removal of molybdate ions from contaminated water and groundwater, Carbohydr. Polym. 180 (2018) 55–62.
[54] B.M. Markovic, Z.M. Vukovic, V.V. Spasojevic, V.B. Kusigerski, V.B. Pavlovic, A. E. Onjia, A.B. Nastasovic, Selective magnetic GMA based potential sorbents for molybdenum and rhenium sorption, J. Alloys Compd. 705 (2017) 38–50.
[55] Y. Ren, P. Liu, J. Feng, J. Ma, Q. Wen, M. Zhang, Selective recognition of molybdenum(VI) from water by Mo(VI) oxy ion-imprinted particle as an adsorbent, Chem. Eng. J. 219 (2013) 286–294.
[56] E. Guibal, C. Milot, J.M. Tobin, Metal-anion sorption by chitosan beads: equilibrium and kinetic studies, Ind. Eng. Chem. Res. 37 (1998) 1454–1463.
[57] A.A. Atia, A.M. Donia, H.A. Awed, Synthesis of magnetic chelating resins functionalized with tetraethylenepentamine for adsorption of molybdate anions from aqueous solutions, J. Hazard. Mater. 155 (2008) 100–108.
[58] E.H. Borai, M.S. Abd El-Ghany, I.M. Ahmed, M.M. Hamed, A.M.S. El-Din, H.F. Aly, Modified acidic leaching for selective separation of thorium, phosphate and rare earth concentrates from Egyptian crude monazite, Int. J. Miner. Process. 149 (2016) 34–41.
[59] H.M. Abdel-Ghafar, E.A. Abdel-Aal, M.A.M. Ibrahim, H. El-Shall, A.K. Ismail, Purification of high iron wet-process phosphoric acid via oxalate precipitation method, Hydrometallurgy 184 (2019) 1–8.
[60] M.F. Hamza, I.E. El-Aassy, E. Guibal, Integrated treatment of tailing material for the selective recovery of uranium, rare earth elements and heavy metals, Miner. Eng. 133 (2019) 138–148.
[61] R.G. Silva, C.A. Morais, L.V. Teixeira, É.D. Oliveira, Selective precipitation of high-quality rare earth oxalates or carbonates from a purified sulfuric liquor containing soluble impurities, Min. Metall. Explor. 36 (2019) 967–977.
[62] Z.S. Abisheva, Z.B. Karshigina, Y.G. Bochevskaya, A. Akcil, E.A. Sargelova, M. N. Kvyatkovskaya, I.Y. Silachyov, Recovery of rare earth metals as critical raw materials from phosphorus slag of long-term storage, Hydrometallurgy 173 (2017) 271–282.